NASA Contractor Report 3898

Convective Storm Downdraft Outflows Detected by NASA/MSFC's Airborne 10.6 μm Pulsed Doppler Lidar System

G. D. Emmitt

CONTRACT NAS8-35597
MAY 1985

NASA

NASA Contractor Report 3898

Convective Storm Downdraft Outflows Detected by NASA/MSFC's Airborne 10.6 μm Pulsed Doppler Lidar System

G. D. Emmitt

Simpson Weather Associates, Inc.
Charlottesville, Virginia

Prepared for
George C. Marshall Space Flight Center
under Contract NAS8-35597

National Aeronautics
and Space Administration

Scientific and Technical Information Branch

1985

ACKNOWLEDGMENTS

The author wishes to acknowledge the support for this research of Mr. John S. Theon and Dr. Robert J. Curran of NASA Headquarters, Washington, DC, and the technical direction of Dr. Daniel E. Fitzjarrald and Mrs. Margaret B. Alexander of the Atmospheric Sciences Division, Systems Dynamics Laboratory and Mr. James W. Bilbro of the Guidance Control and Optical Systems Division, Information and Electronics Laboratory, Marshall Space Flight Center, Alabama.

TABLE OF CONTENTS

Convective Storm Downdraft Outflows Detected by NASA/MSFC's Airborne 10.6 μm Pulsed Doppler Lidar System

1.0 INTRODUCTION

In the summer of 1981 the NASA/MSFC's 10.6 μm CO_2 Pulsed Doppler Lidar System was mounted in a NASA CV990 aircraft as part of a program to demonstrate and evaluate the lidar's capability to provide two dimensional wind fields in a variety of atmospheric and topographical situations. Engineering details and some preliminary examples of the wind data obtained have been compiled in a document by Bilbro, et al., 1984. The aircraft operation is illustrated in Figure 1 and the pattern of lidar shots that permits an estimation of the 2-D wind field is shown in Figure 2.

To intercept storm outflows, the CV990 was flown ~400 m (AGL) and within 5-10 km of the edge of the targeted convection. Some of the system parameters remained nearly constant for all the outflow experiments:

pulse length	330 m
aircraft true airspeed	260-300 knots
aircraft altitude	400-600 m AGL
lidar range	8-12 km

Except for system biases (which have been removed) each wind vector estimated for a 330 m x 330 m square is totally independent of neighboring wind estimates. Unless noted, no smoothing of the wind field is made. Therefore, the coherence of the wind field estimates is a partial indication of the lidar system performance.

Participation in CCOPE provided NASA an opportunity to evaluate the airborne lidar with the benefit of several sources of complementary and supplementary observations such as radars, a rawinsonde network, a surface station network, satellite imagery coverage and other aircraft measurements (Figure 3). The following case studies attempt to bring together the Airborne Doppler Lidar System (ADLS) wind measurements with these other observations to demonstrate the flow visualization that is possible in regions of a storm that are not easily accessed by previously available observational tools. Where appropriate, physically significant conclusions are made; however, these are mostly limited to kinematics because of the lack of temperature and moisture measurements on time and space scales commensurate with those of the lidar.

All of the CCOPE ADLS data were reviewed for measurements in the sub-cloud region of active cumulus convection. On the 21st and 23rd of July 1981 there were several cases when the CV990 was flown in a manner very similar to that shown in Figure 1. In total, nearly 600 km (x 10 km) of storm outflow data were collected on Flights 16 and 17. In order to put these data in the context of the general atmospheric conditions, synoptic maps, radar maps, surface network data, and satellite imagery were consulted. The net result is a set of unique visualizations of flows within the sub-cloud region, substantiated on a few occasions by available comparisons with more conventional wind measuring systems.

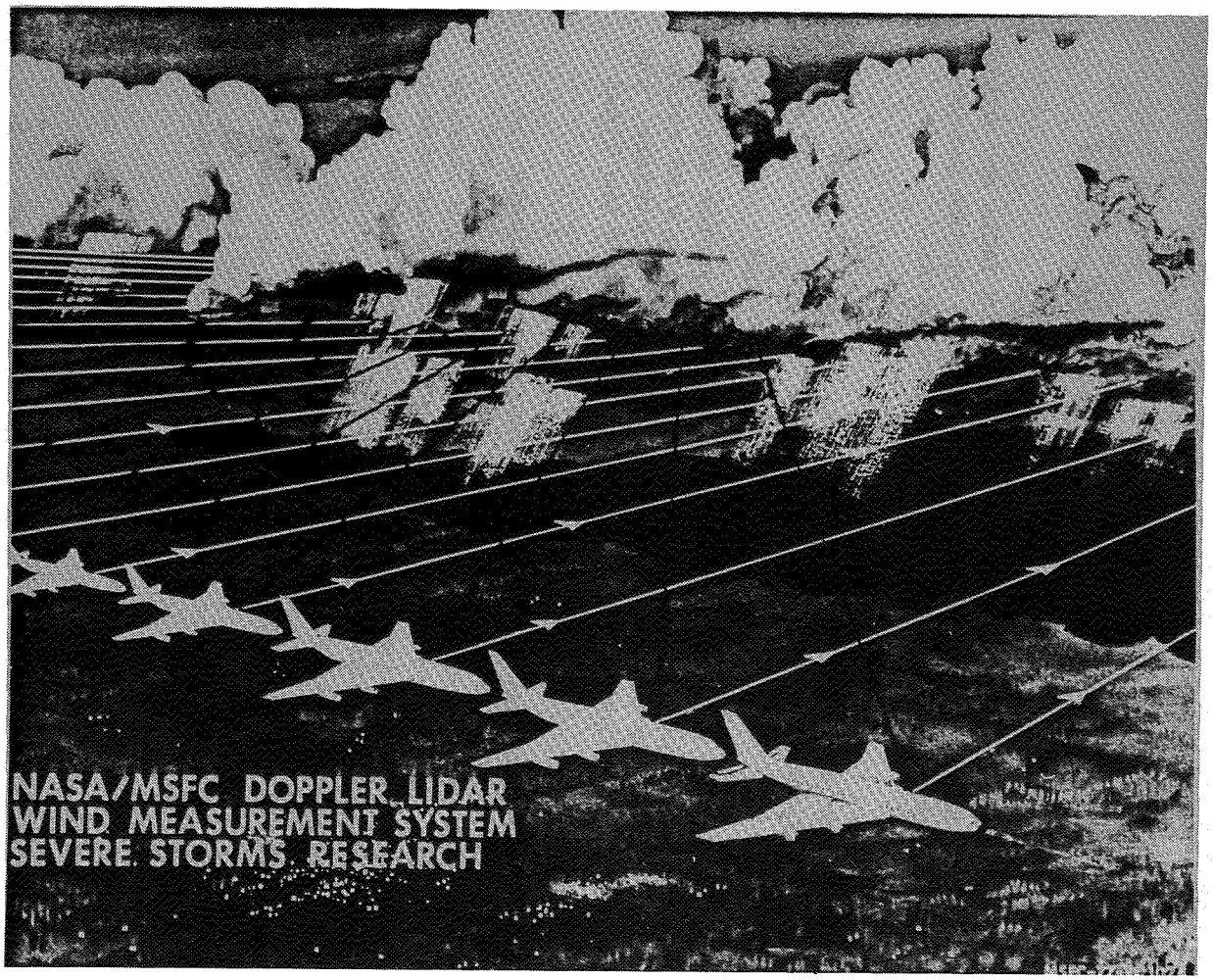

Fig. 1. Illustration of a severe storm outflow Airborne Doppler Lidar mission. The CV990 aircraft flies approximately 400 m above ground level (AGL) with a ground speed between 275 and 300 kts. "Forward" (20^{o} from the cross track direction) and "Aft" (also 20^{o}) lidar scans are made alternately and about 1 second apart. See Figure 2 for more details.

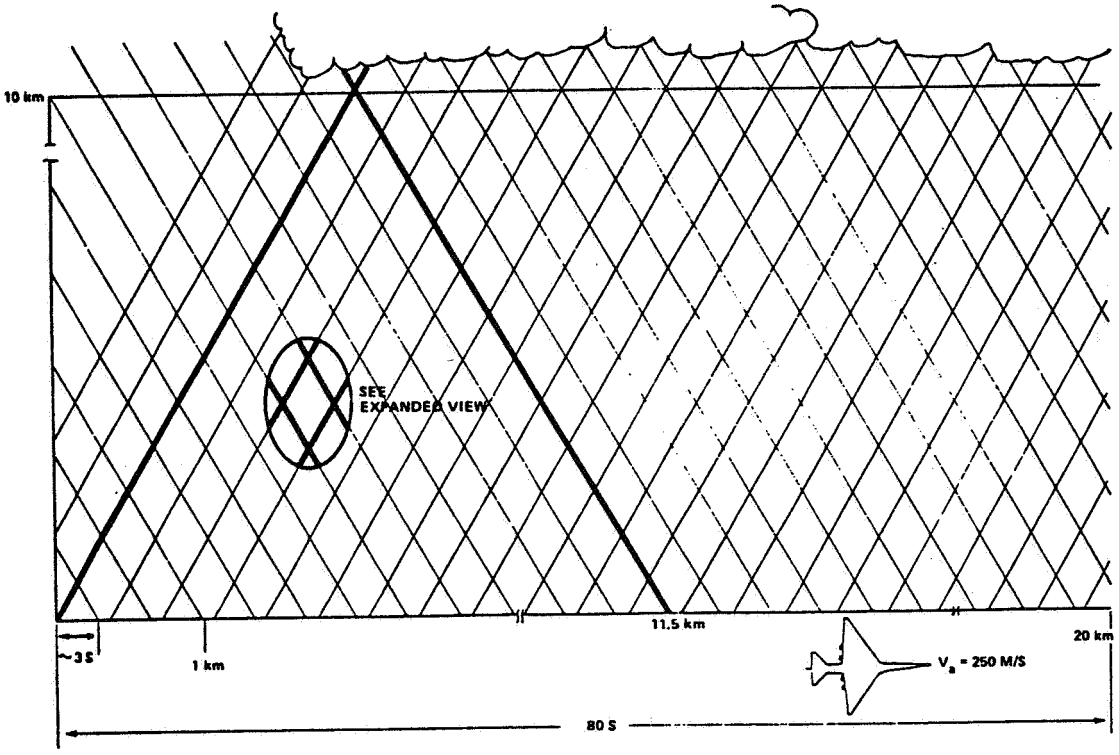

Fig. 2. A. Airborne Doppler lidar scan pattern.

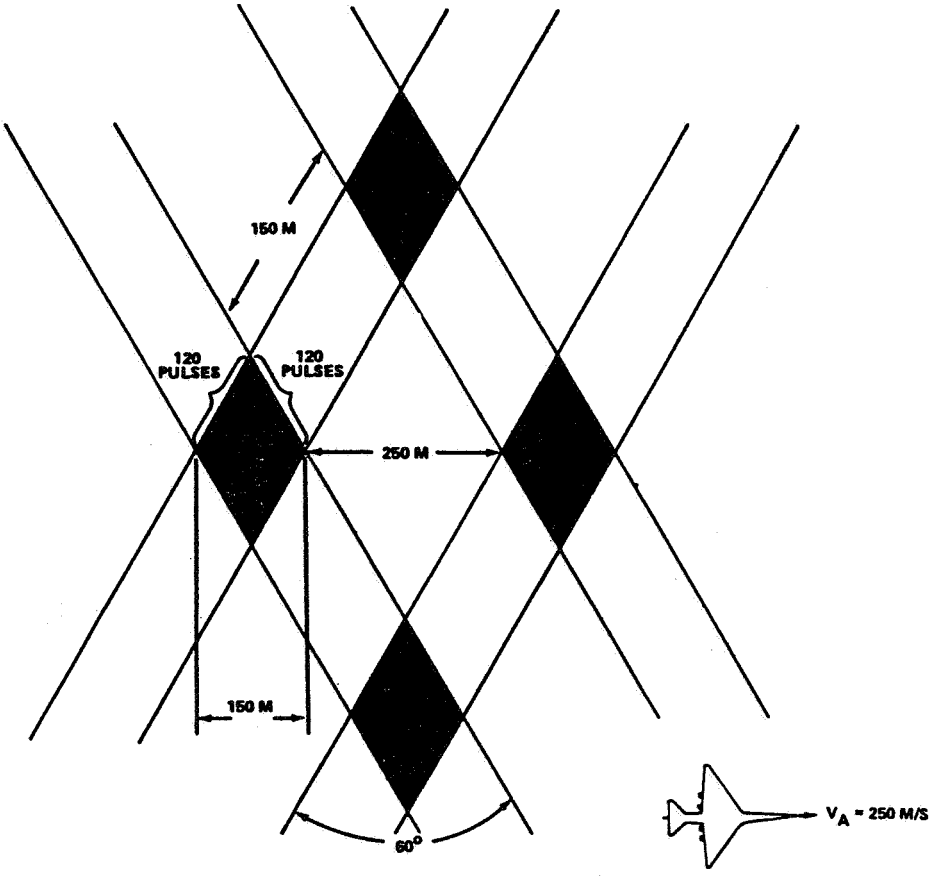

B. Expanded view of scan pattern.

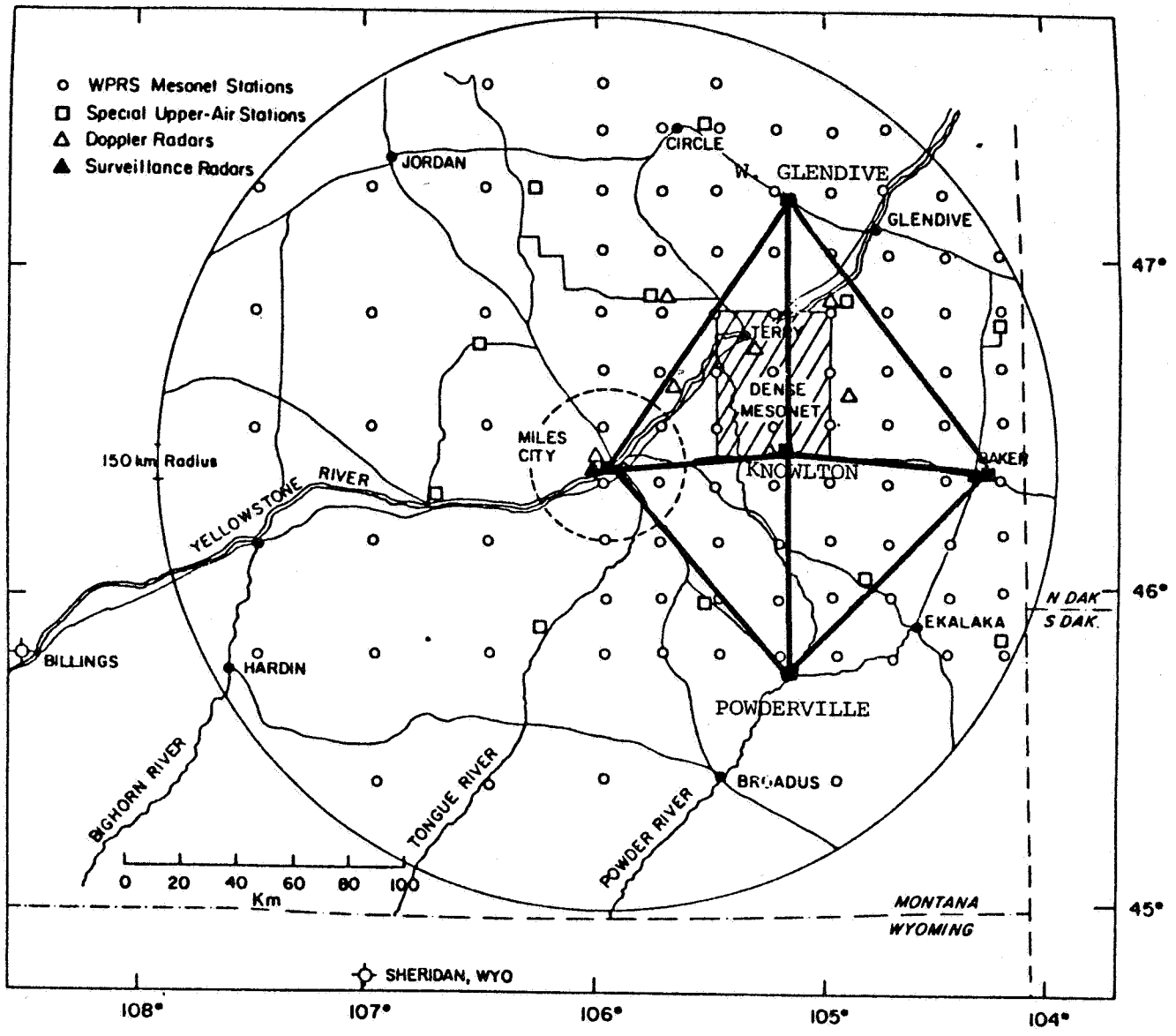

Fig. 3. Locations of special observing networks in CCOPE. Taken from the CCOPE Preliminary Experiment Design Document.

2.0 CASE STUDIES

2.1 July 21, 1981

Convective storm outflows were the primary targets of this flight mission. As shown in Figure 4, the interesting parts of the flight occured just on or beyond the northeastern edge of the surface network thus minimizing the usefulness of the surface network data. The satellite imagery does, however, provide the cloud field context for the flight paths analyzed (Figure 5). The precise navigation of aircraft data relative to the satellite data has not been fully pursued. The benefits of such an effort would be minimal since the cirrus cover prevents any detailed matching of the lidar derived wind fields with individual cumulus features.

2.1.1 Synoptic Situation

The following is a quote from the 21 July CCOPE operational morning forecast: "Air mass dry in low levels but steep temperature lapse rate. A trough along the east border (of study area) should provide trigger for TCU/CB NE-E (could be out of area). Mid-level ACCAS is interesting and could build significantly by late afternoon." This forecast turned out to be basically correct with most of the deep convection to the E and NE of the CCOPE surface network.

2.1.2 Storm Characteristics

A Radar time history

Figure 6 presents the SWR-75 echo time history between 2300 and 0015 ZST. During that time period the storm system went through a cycle of 50-60 dbz maximums to <40 dbz maximums and then back to 50-60 dbz maximums. The western ends of runs 11, 12 and 13 are just on the edge of the 150 km radar range limit.

B Surface Network Observations

Unfortunately this storm was intercepted when it was just on the northeastern edge of the CCOPE surface network. In Figure 7 a streamline analysis at 2315 Z indicates a line of divergent flow originating about 20 km to the north of the CV990 flight track (Flight 16 Run 11). Although the alignment is not perfect, the center of the divergence appears to be associated with the cold pools of air just on the network boundary and the presence of strong radar returns (55 dbz) from convection just north of the area. All these facts are consistent with the perception of the scientific observers onboard the CV990 that a rather active storm with strong outflows was being sampled.

The next time the CV990 was back over the CCOPE network was during the first part of Run 13 (Figure 8). The flight track was directly over an outflow region seen as a core of divergence within

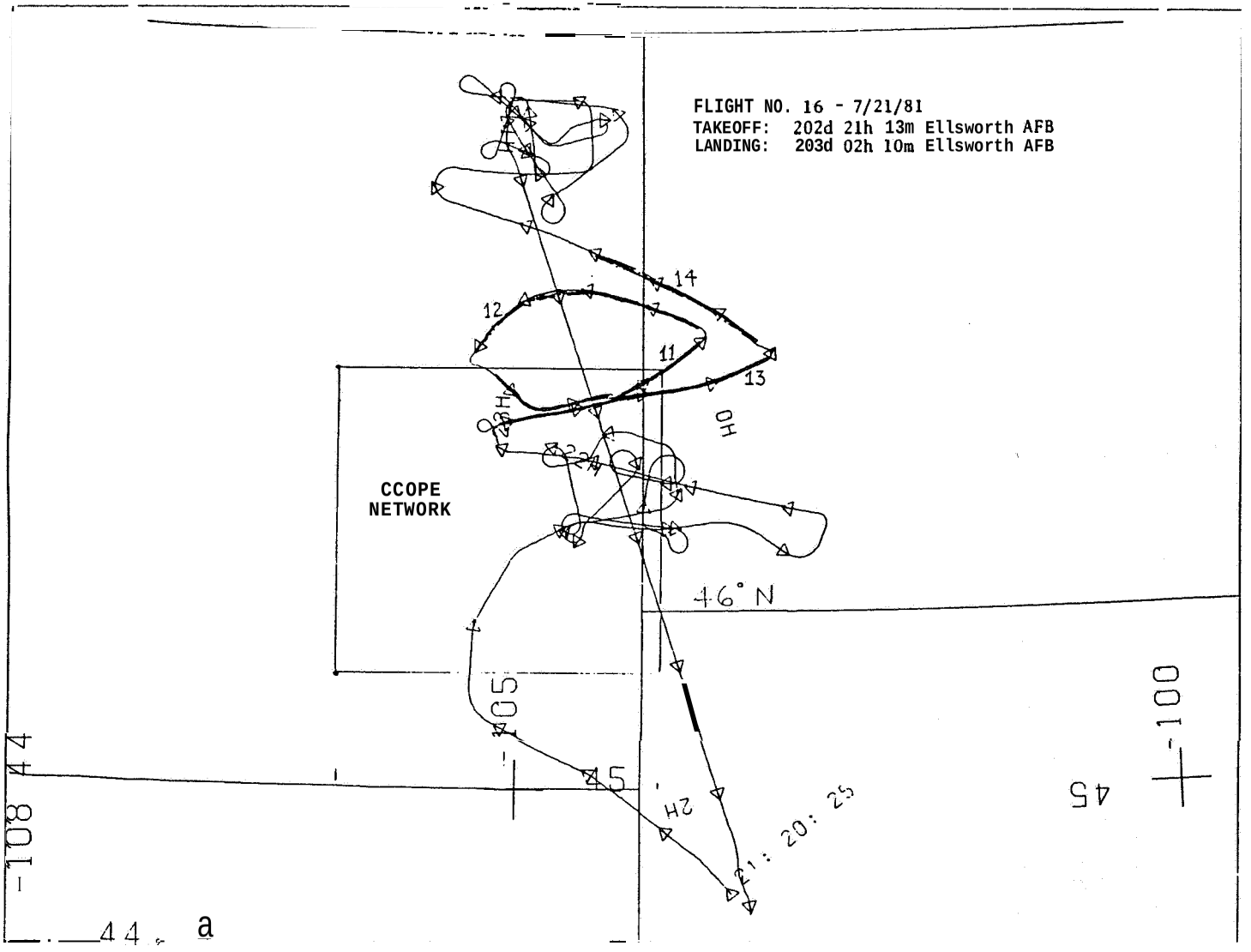

Fig. 4. CV990 ground track duriny Flight 16 on the 21 July 1981 during the CCOPE. The darker sections of the track are used in the case studies presented in this document. The CCOPE surface network is outlined for reference.

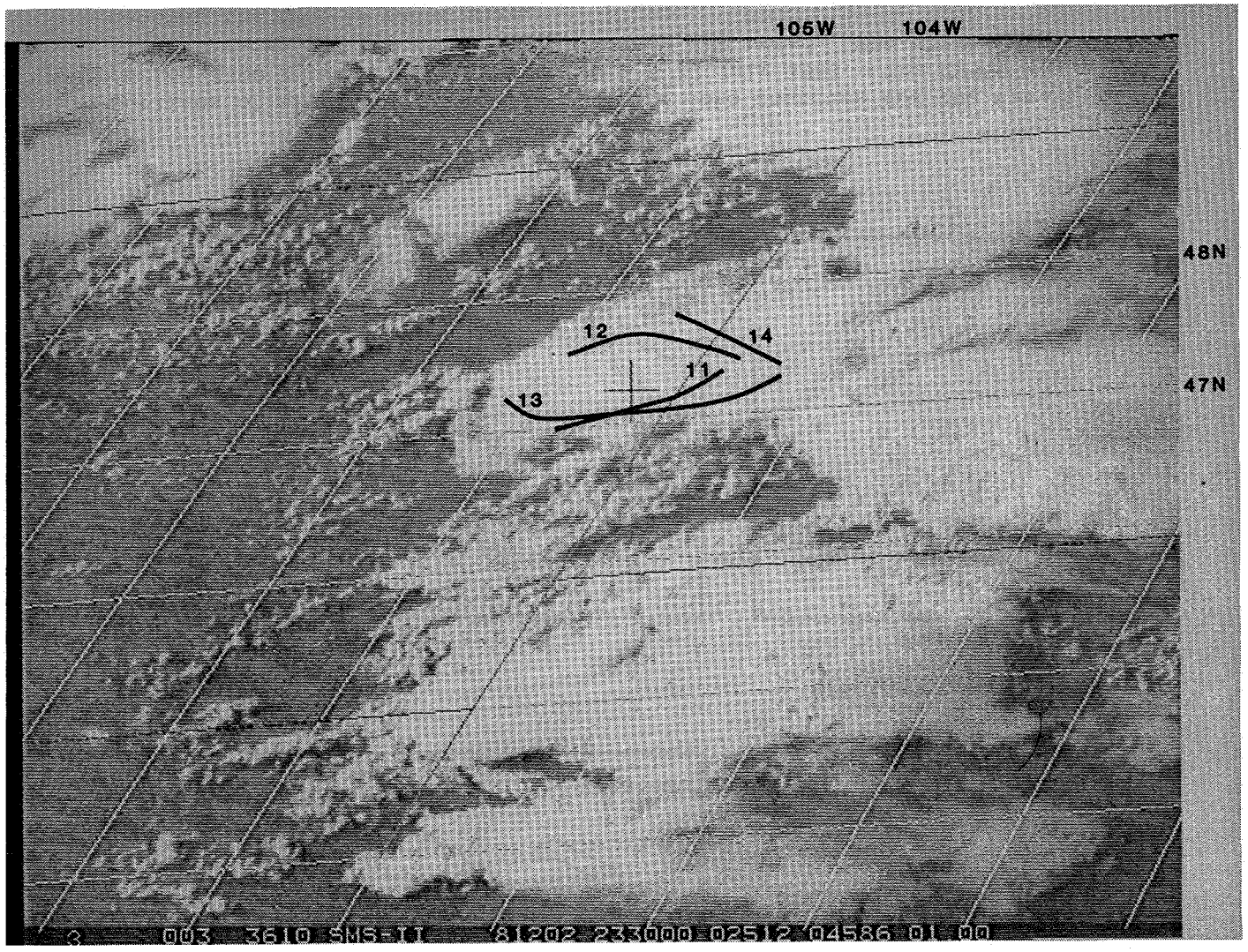

Fiq. 5. Visible **GOES** E imagery for 2330 Z on 21 **July** 1991. CV990 fliyht tracks **for** ADL runs 11, 12, 13 and 14 are superimposed. Latitudes **and** longitudes are noted on the margins of the image.

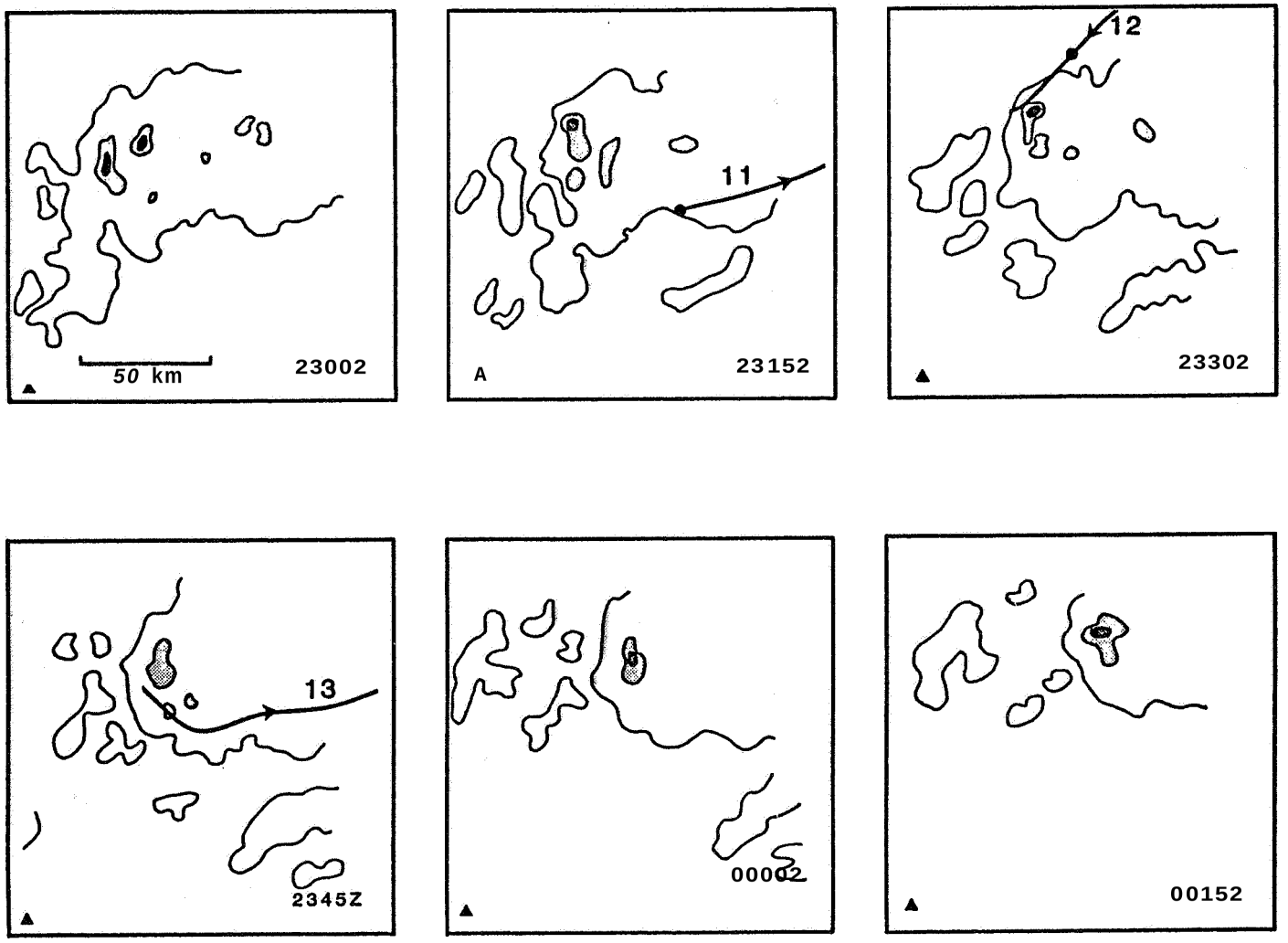

Fig. 6. Outlines of the 30, 40, and 50 dbz radar echo contours for the time period 2300 Z on 21 July 1981 to 0015 Z 22 July 1981. The CV990 flight tracks for the given time windows are noted. The black A denotes the SWR-75 radar site.

GRID SPACING: 5.36 KM

MONTANA MESOSCALE NETWORK DATA
5 MINUTE AVERAGE PRIOR TO 81 07 21 2315 Z

_____STREAMLINES
_ _ _ _TEMPERATURE (C)

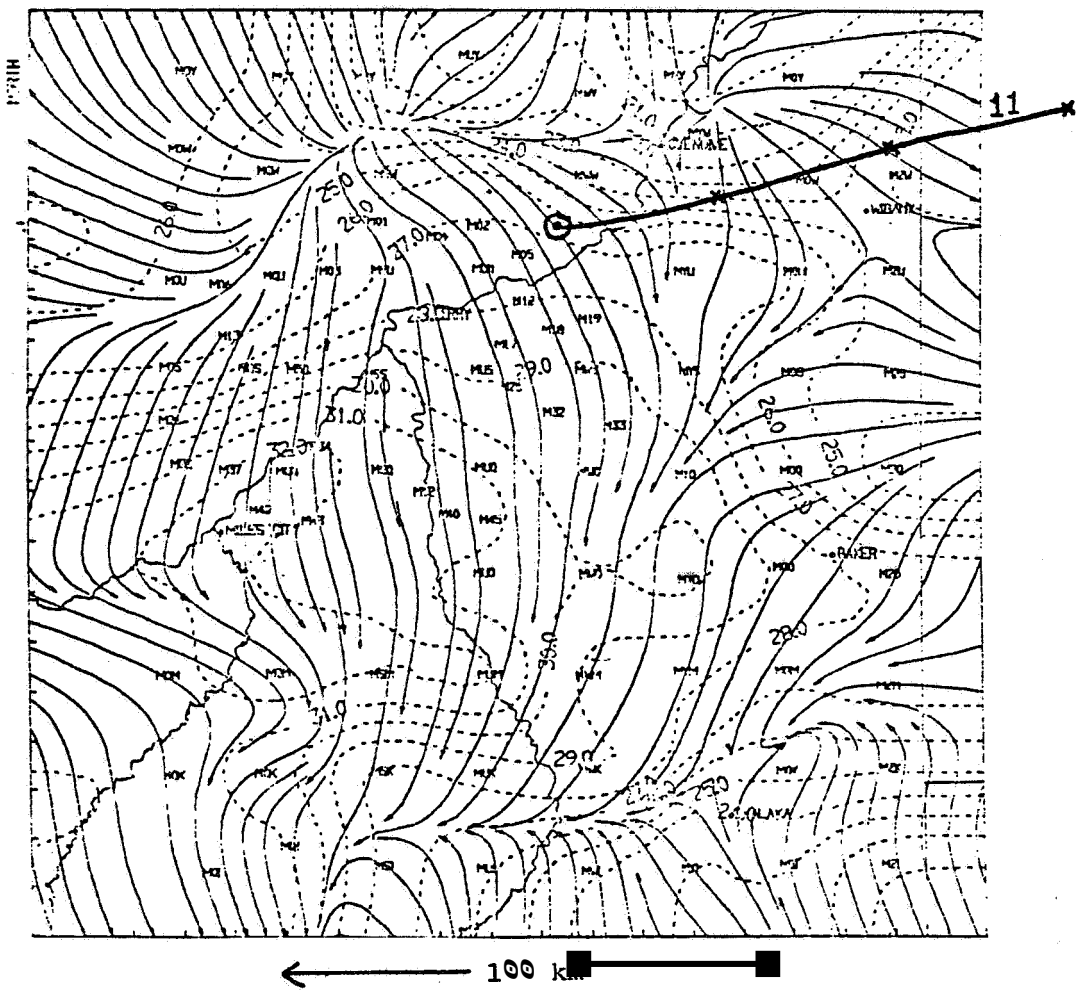

Fig. 7. CCOPE Mesoscale Network streamline (——) and temperature (----) fields for 2315 Z on 21 July 1981. Both E-W and N-S scale are 1" = 17.5 km.

GRID SPACING: 5.36 KM

MONTANA MESOSCALE NETWORK DATA
5 MINUTE AVERAGE PRIOR TO 81 07 21 2345 GMT

STREAMLINES
DIVERGENCE (E-4 SEC-1)

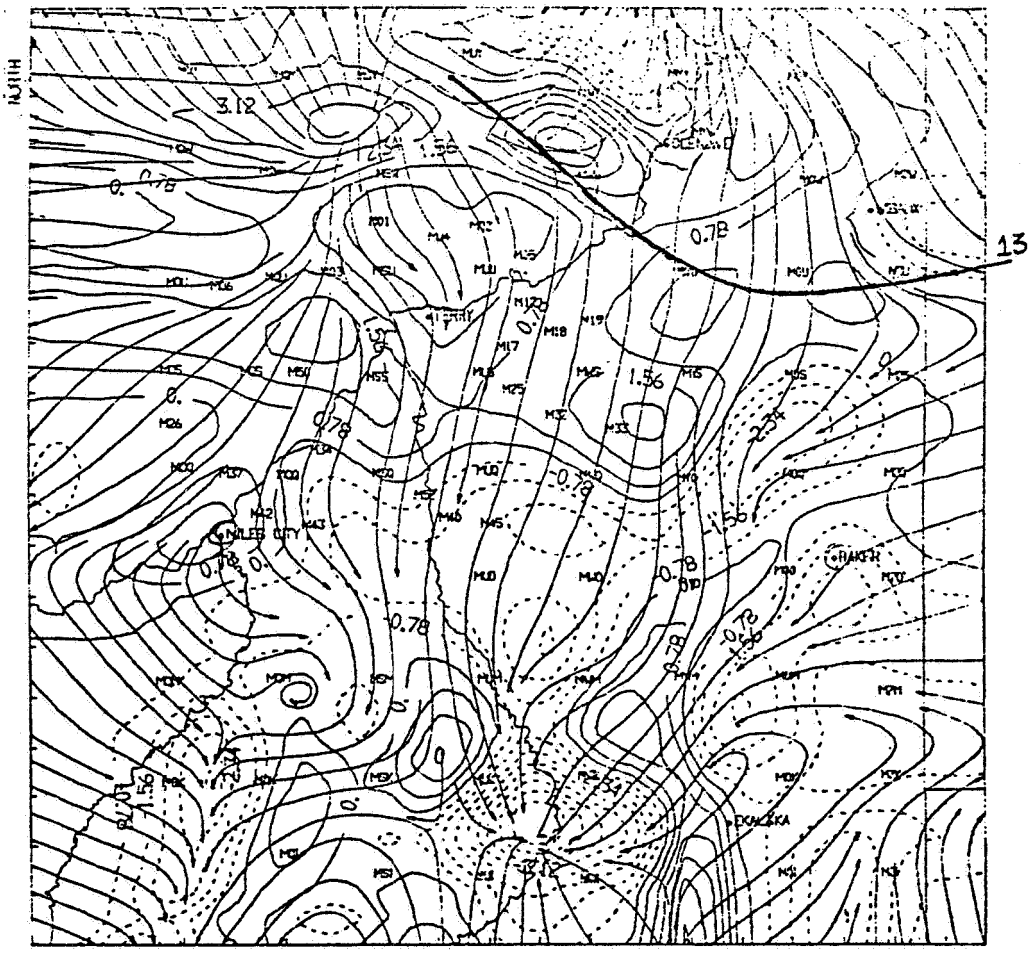

Fig. 8. CCOPE Mesoscale Network streamline (——), divergence (——) and convergence (----) fields for 2345 Z on 21 July 1981. 1" = 17.5 km.

the surface network and associated with a 50-60 dbz radar echo (Figure 6).

C Satellite Imagery

A review of the satellite visible and IR imagery for the period 1600-0200 Z indicated that the storm complex targeted for observations by the DLV was becoming organized around 1930-2000 Z, nearly 3.5 hours before the aircraft measurements (Figure 9). The storm system moved ENE and by 0200 was completely out of the CCOPE network and had become a part of a much larger complex stretching from Nebraska through the Dakotas (Figure 10). A visible image (2330 Z) taken during the time the DLV was in operation was shown in Figure 5. The cirrus obscures the detail of the convective cells and their organization, making it impossible to be precise in associating any ADLS wind flow with the responsible cumulus tower.

D Airborne Doppler Lidar System

The CV990 arrived on the SW flank of the storm at 2305 Z and then flew four separate runs (11, 12, 13 and 14) which encircled the most active (western) portion of the convective system (See Figure 5). To facilitate the discussion of the ADLS wind fields, three levels of display are used. For general flow features, the full resolution (330 meters) data set is averaged over a 2 km grid. Divergence and vorticity fields are also calculated at this resolution. Higher resolution divergence and vorticity fields are available with 1 km averaging--and are presented on a selective basis. For the highest resolution of the wind vector fields, the .33 km data with no smoothing is used. This full resolution product provides evidence of how consistent the wind vector estimates are in the presence of flow features such as storm outflows.

Looking back at Figures 7 and 8 we see a boundary layer flow dominated by centers of convergence and divergence which are expected in the presence of deep convection. As the CV990 flew around the NE corner of the CCOPE surface network, the general sense of the flow at 450 m AGL was from WNW on the southern legs (11 and 13) and from SSE along the northern legs (12 and 14). This is consistent with the difluent flow seen with surface network during the period 2300-0015 Z.

In Figure 11 (2 km averaged winds for run 11) four flow features are identified. At location A the winds dropped from 20-30 kts to <4 kts. This was followed by a 15 km wide northerly flow (B) of 15-20 kts with a $1^{o}C$ temperature drop (measured on the aircraft) and then a return to 20-30 kts westerlies. At C there was again a weak northerly intrusion, followed by the strong westerlies. In area D there occurs one of the strongest perturbations seen on the outflow flights. The 1 km averaged wind, divergence and vorticity fields are shown in Figure 12. In general, there is convergence (negative numbers in 12B) ahead of the outflow, divergence inside its boundaries, and vorticity of both signs along its edges. The limit of meaningful values is around 10-12 km from the aircraft.

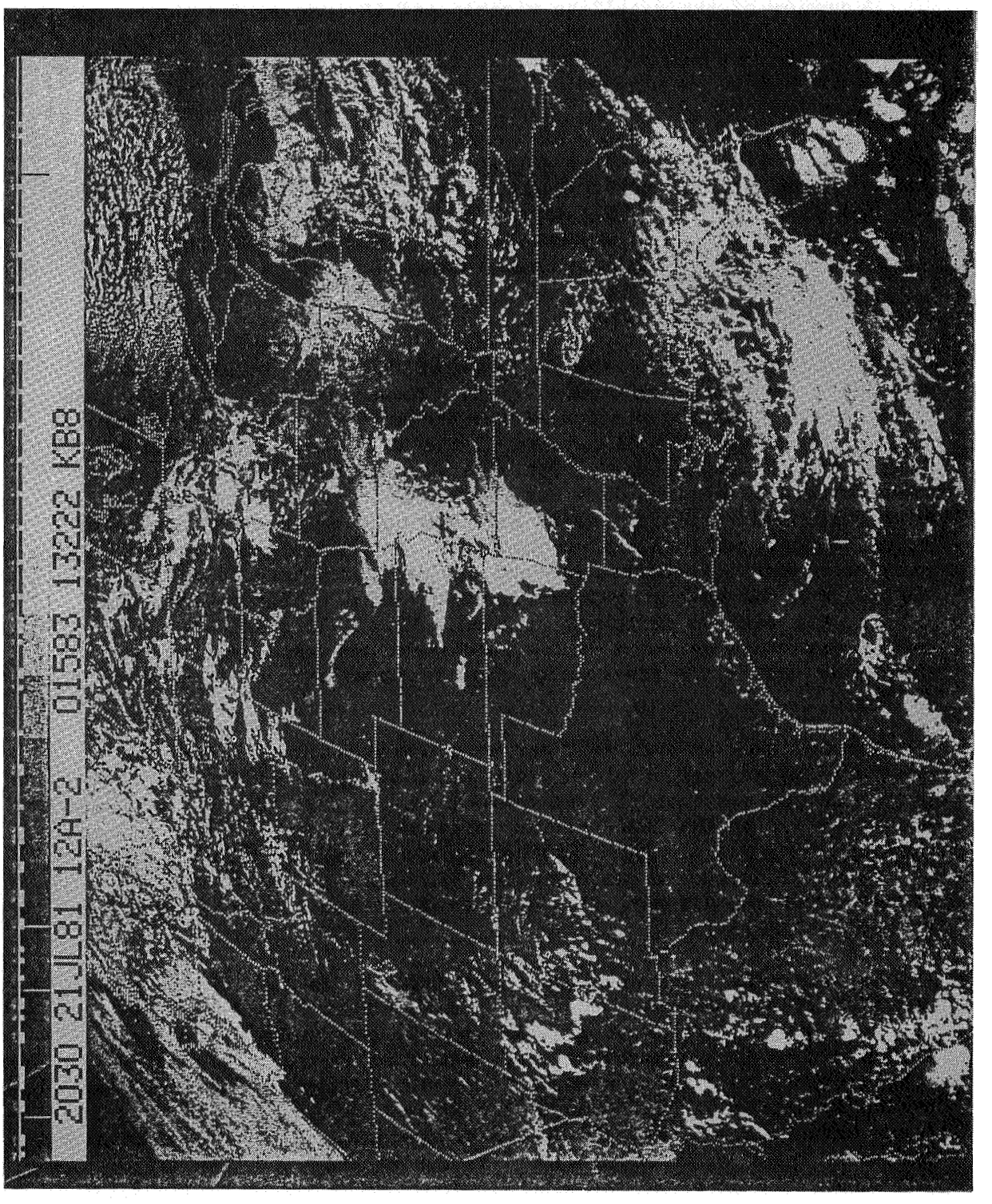

Fig. 9. GOES E **visible image for 2030 Z, 21 July 1981.** CCOPE **network is in east central Montana.**

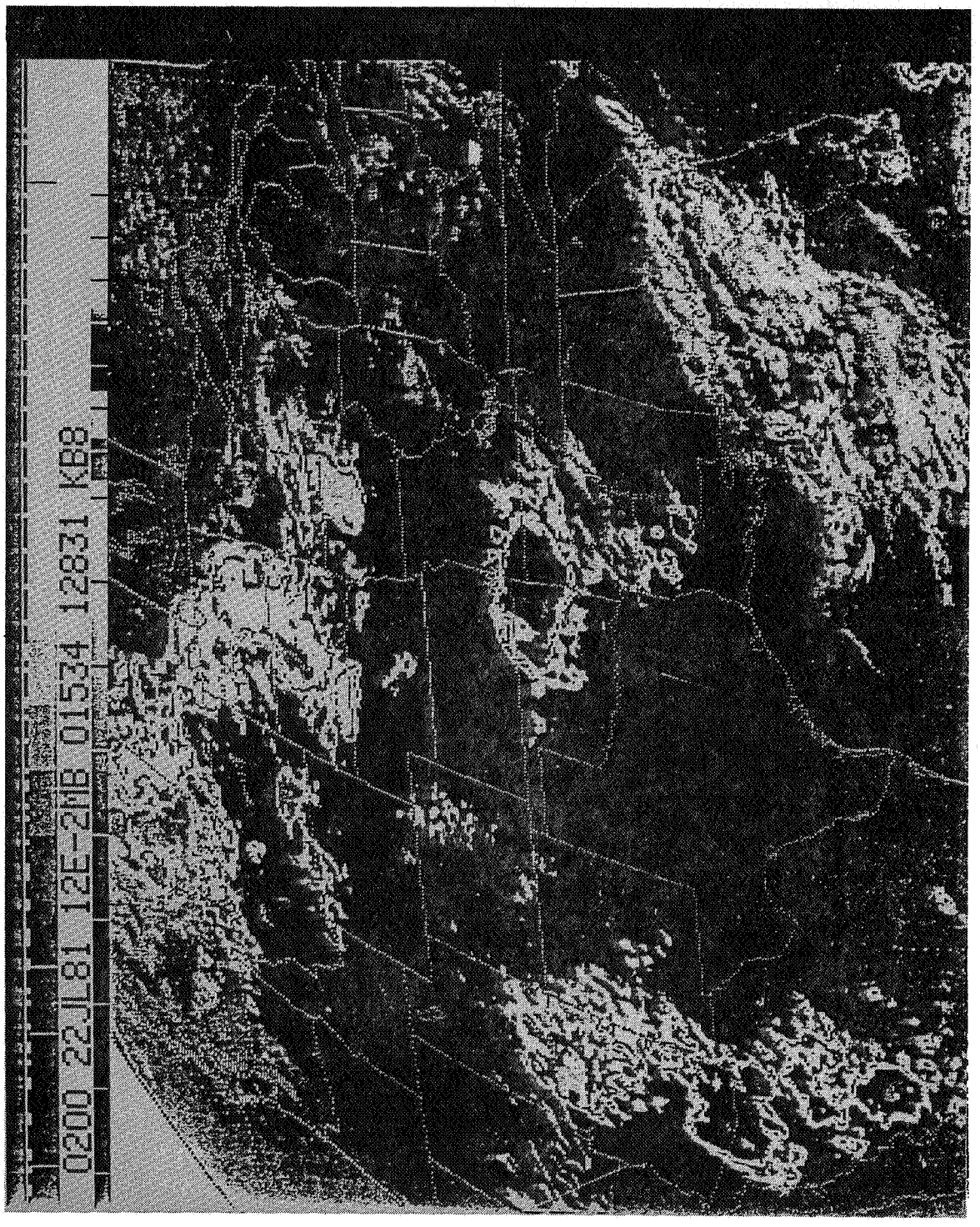

Fig. 10. GOES E infrared image for 0200 22 July 1901. Most of deep convection has moved out of the CCOPE network in east central Montana.

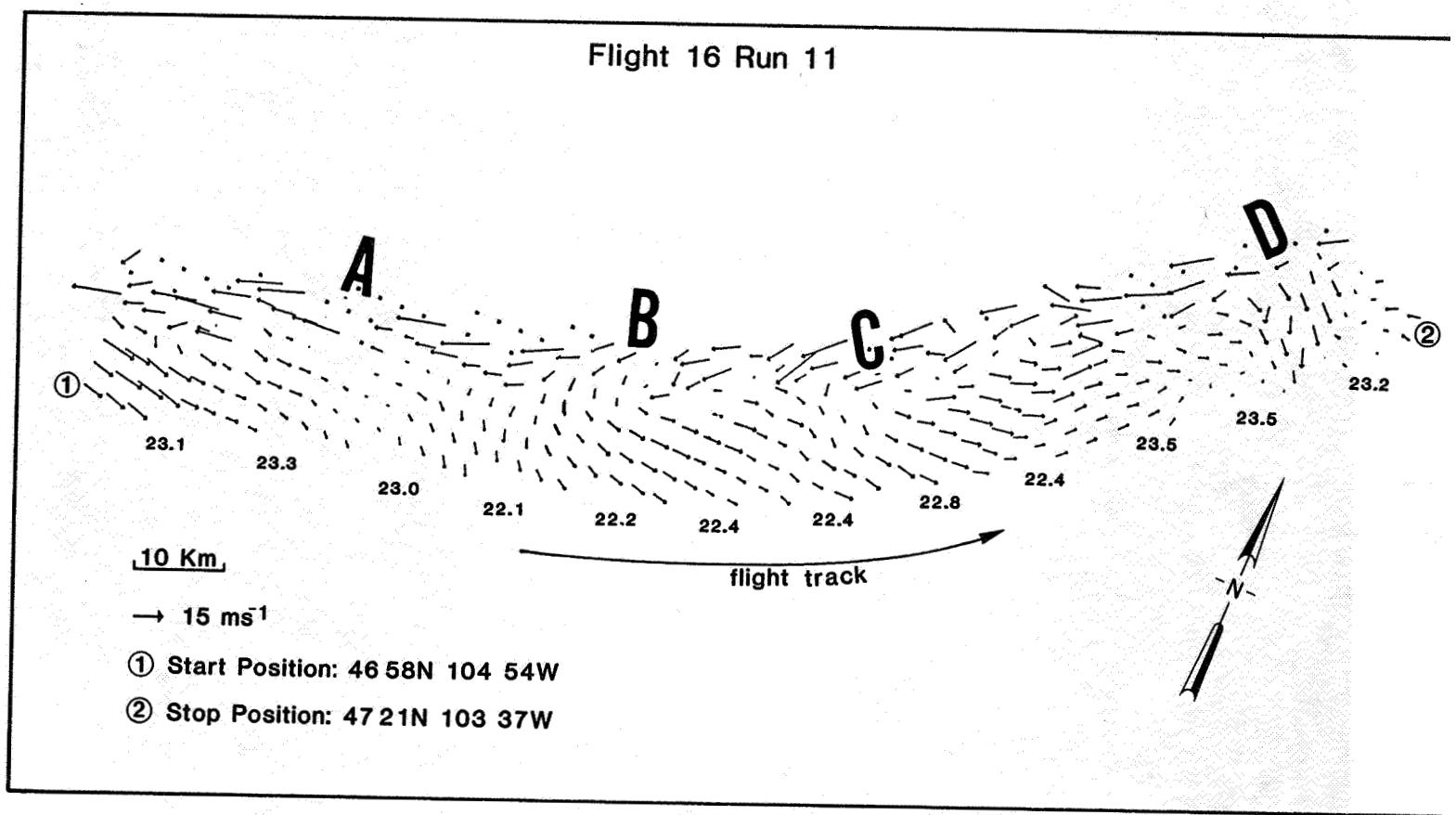

Fig. 11. Airborne Doppler Lidar winds obtained during Flight 16 run 11 (2309 - 2320 Z) on 21 July 1982. Wind vectors represent averages of the 330 m wind data over 2 km squares. The numbers along the aircraft track are static temperatures measured on the CV-990.

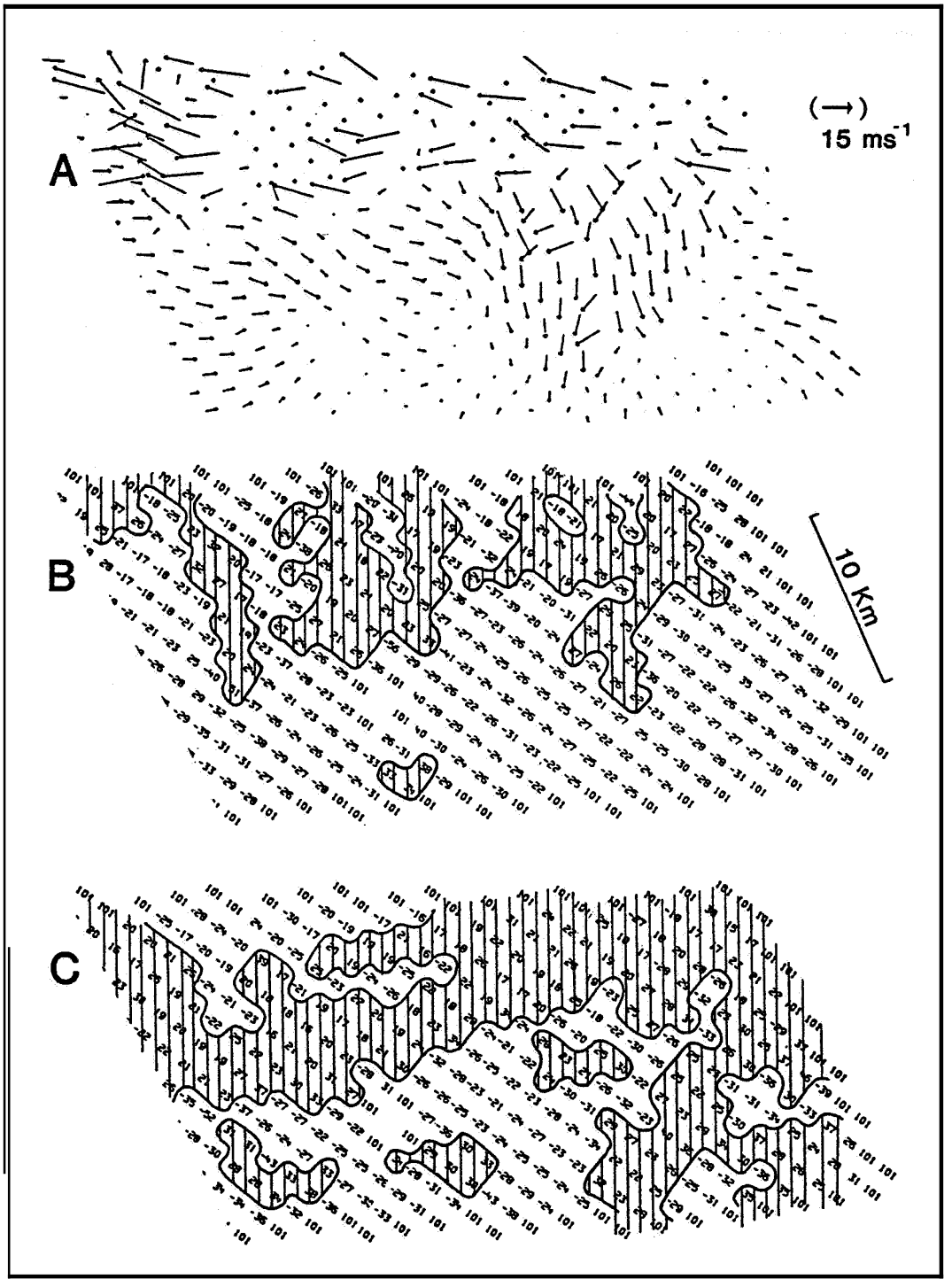

Fig. 12 Airborne Doppler Lidar wind (12A), divergence (12B), and vorticity (12C) fields obtained near feature D in Figure 11 during Flight 16, Run 11 on 21 July 1981. Vector and scalar fields are 1 km averages of the 330 meter full resolution data set. The $\log_{10}$ (x 10) of the divergences and vorticities are displayed with the sign denoting the sense of the differentials (i.e. -25 in the divergence data is to be interpreted as $-1.0 \times 10^{-2.5}$ s^{-1}. Likewise 35 represents $1.0 \times 10^{-3.5}$ s^{-1}.) Areas of divergence (or positive vorticity) are hatched.

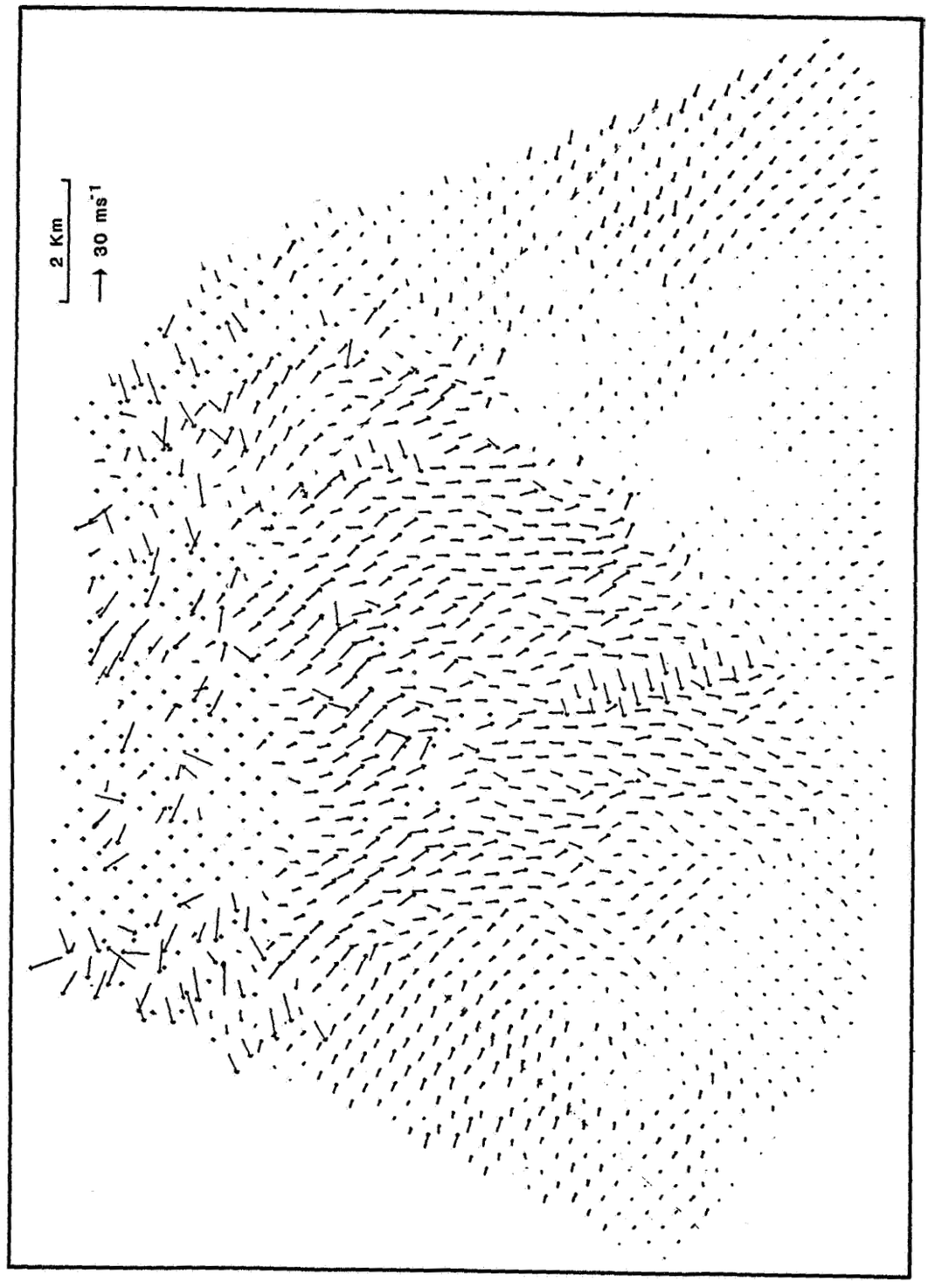

Fig. 13. Full resolution (330 m) ADL wind data for feature D in Figure 11.

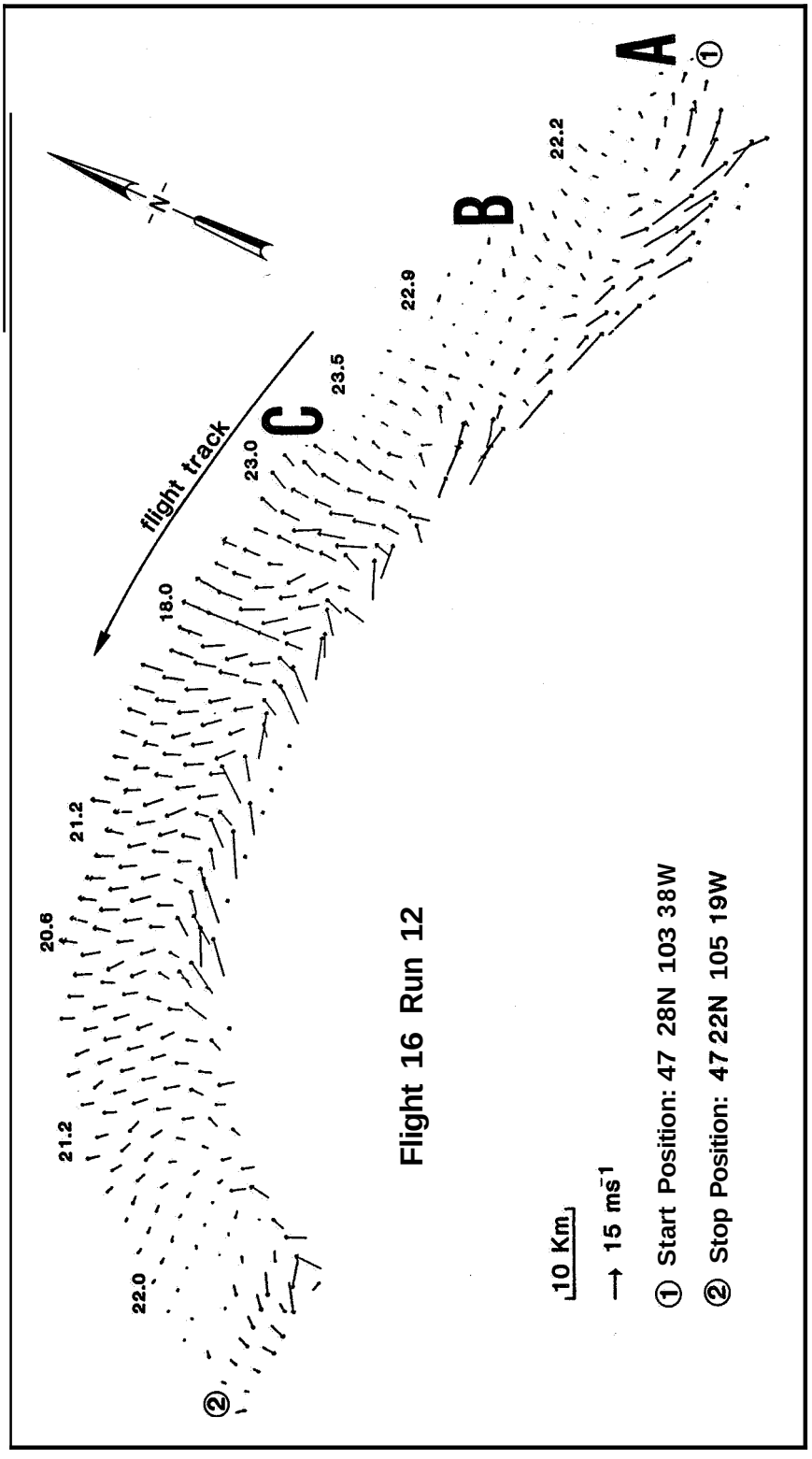

Fig. 14. Airborne Doppler Lidar winds obtained during Flight 16 Run 12 (2323 - 2336 Z) on 21 July 1981. Wind vectors represent averages of the 330 m ADL wind data over 2 km areas. Temperatures measured onboard the NASA CV990 are presented along the aircraft flight track.

Although the kinematic picture presented by the lidar data is not unexpected and conforms to our general understanding of storm outflows, this case demonstrates the consistent nature of the Doppler lidar wind measurements in the vicinity of significant flow structures. Even without any averaging (Figure 13), the individual and independent wind estimates provide a coherent and immediately interpretable presentation of the horizontal wind fields. The full resolution display also alerts one to the occurrance of large and not always random errors that could produce not so obvious errors in the averaged fields.

For Run 12 (400-600 meters AGL) the CV9900 turned to a WNW heading and tried to stay just to the north of the main convection. In Figure 14 three features are labeled. Within region A there is the general background westerly flow of 10-12 kts. In Region B we see a relatively weak (7-8 kts) northerly flow with a shape similar to that of feature D on Run 11. The aircraft temperature probe data are provided along the flight track. From these data the flow at B is seen to be slightly cooler (-.6^{o}C) than the air to the east and west of it. The edge of a stronger outflow is labeled as C. Fifteen km to the west of point C the aircraft measured temperature drops 5.5^{o}C and the aircraft INS winds increase to 28-32 kts from the SSW. The lidar was measuring 30 kts in the same area. For the next 50 km the flow remained strong (>15 kts) and slowly backed from SSW to SSE. This pattern is consistent with a downdraft outflow from the convective complex detected by the SWR-75 radar.

A closer examination of the outflow boundary at point C in Figure 14 is provided in Figure 15 where the 1 km vector, divergence and vorticity fields are displayed. Note the strong convergences as the northerly outflow runs into the generally westerly flow and also the generation of an extensive (200 - 400 km^{2}) area of negative vorticity.

After flying around the western edge of the storm, Run 13 began with the CV990 on a heading of 135^{o} and at an altitude of 400 meters AGL. The 2 km average wind field is presented in Figure 16. Although there are many details in the flow, two features have been singled out for high resolution. In region A there is a collision of a strong westerly flow (25-30 kts) with a weaker (15-20 kts) but organized northerly flow. The 1 km wind vector, divergence and vorticity fields in this region are shown in Figure 17. As annotated in Figure 17, the aircraft temperature sensors measured little change in temperature at this intersection.

In region B there is another zone of convergence which is shown in 1 km resolution (Figure 18). Once again there is significant structure in the wind field without an obvious correlated horizontal temperature structure. Around the southern edge of the storm, the strong winds at 500 m AGL appear to be more westerly with distance from the radar echo region. Without knowing the thermal and kinetic fields below the flight level, it can be only conjectured that the outflows may be shallow and quite cold with strong decoupling from the overlying air. This decoupling could lead to accelerations in

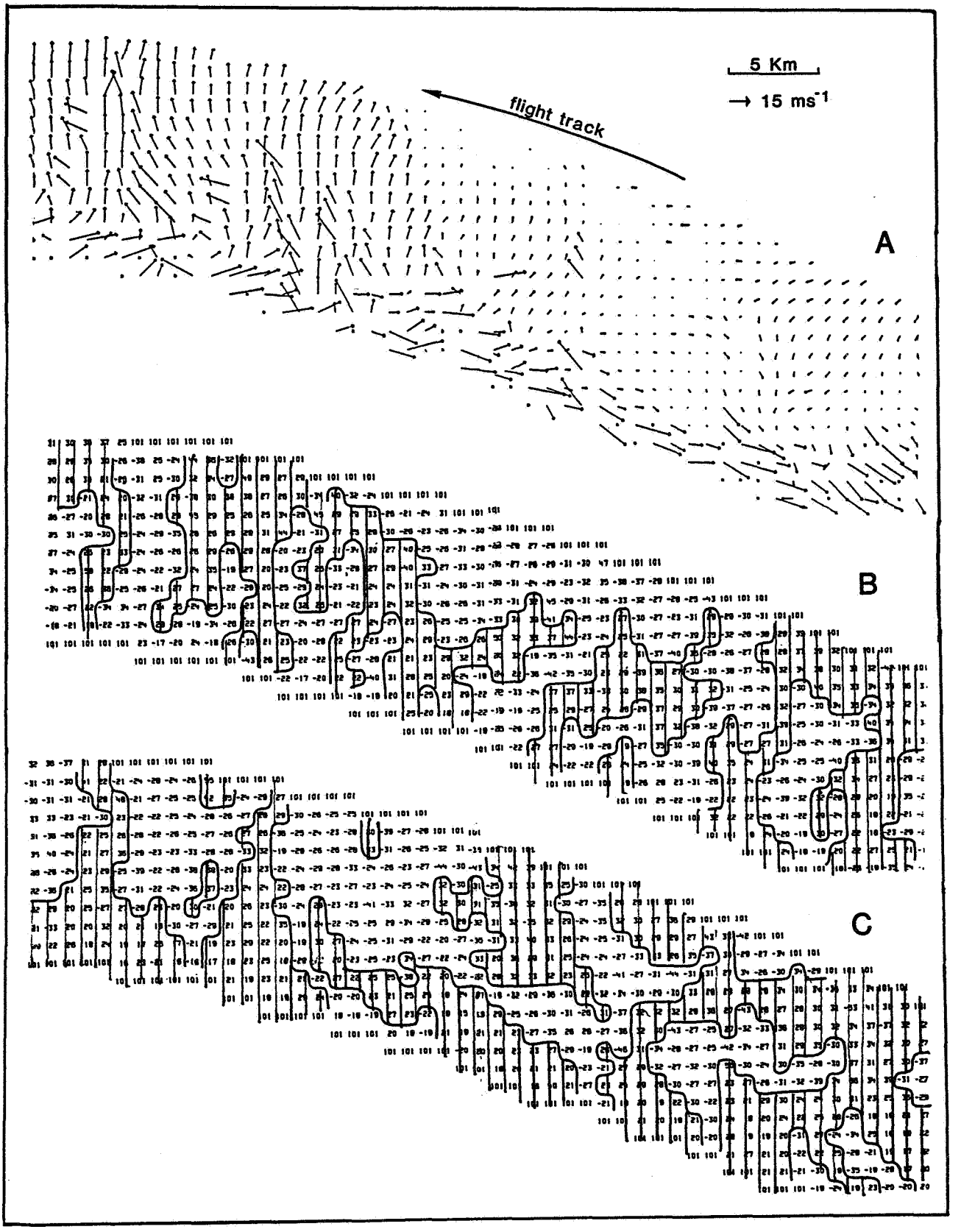

Fig. 15. Airborne Doppler Lidar 1 km averaged wind vectors (15A), divergence (15B), and vorticity fields (15C) for feature C in Figure 14. See Figure 12 caption for further explanation.

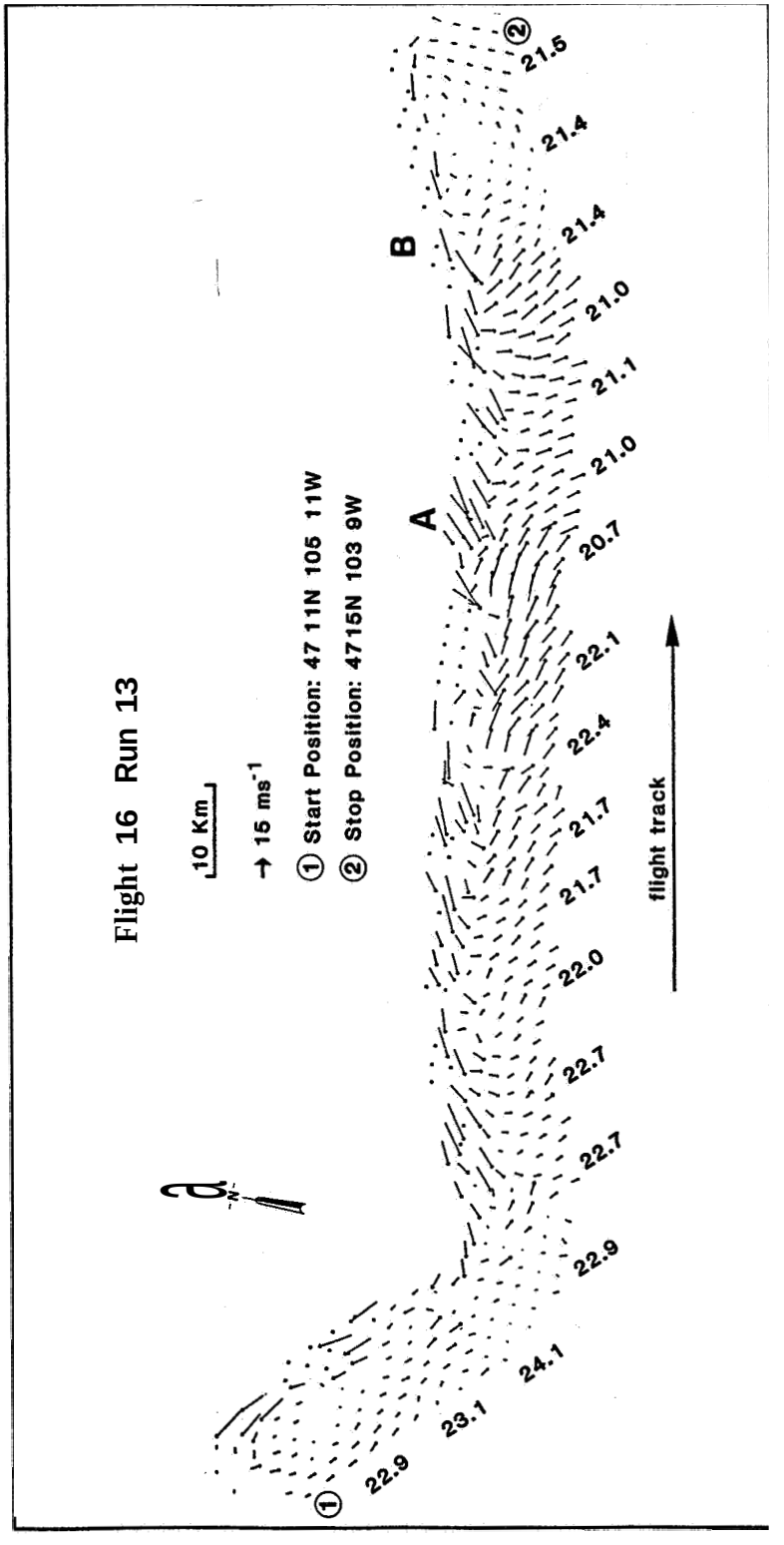

Fig. 16. Airborne Doppler Lidar winds obtained during Flight 16 run 13 (2346 - 0003 Z) 21-22 July 1981. Wind vectors represent 2 km averages of the full resolution (330 m) wind data. Temperatures measured onboard the NASA CV990 are presented along the aircraft flight track.

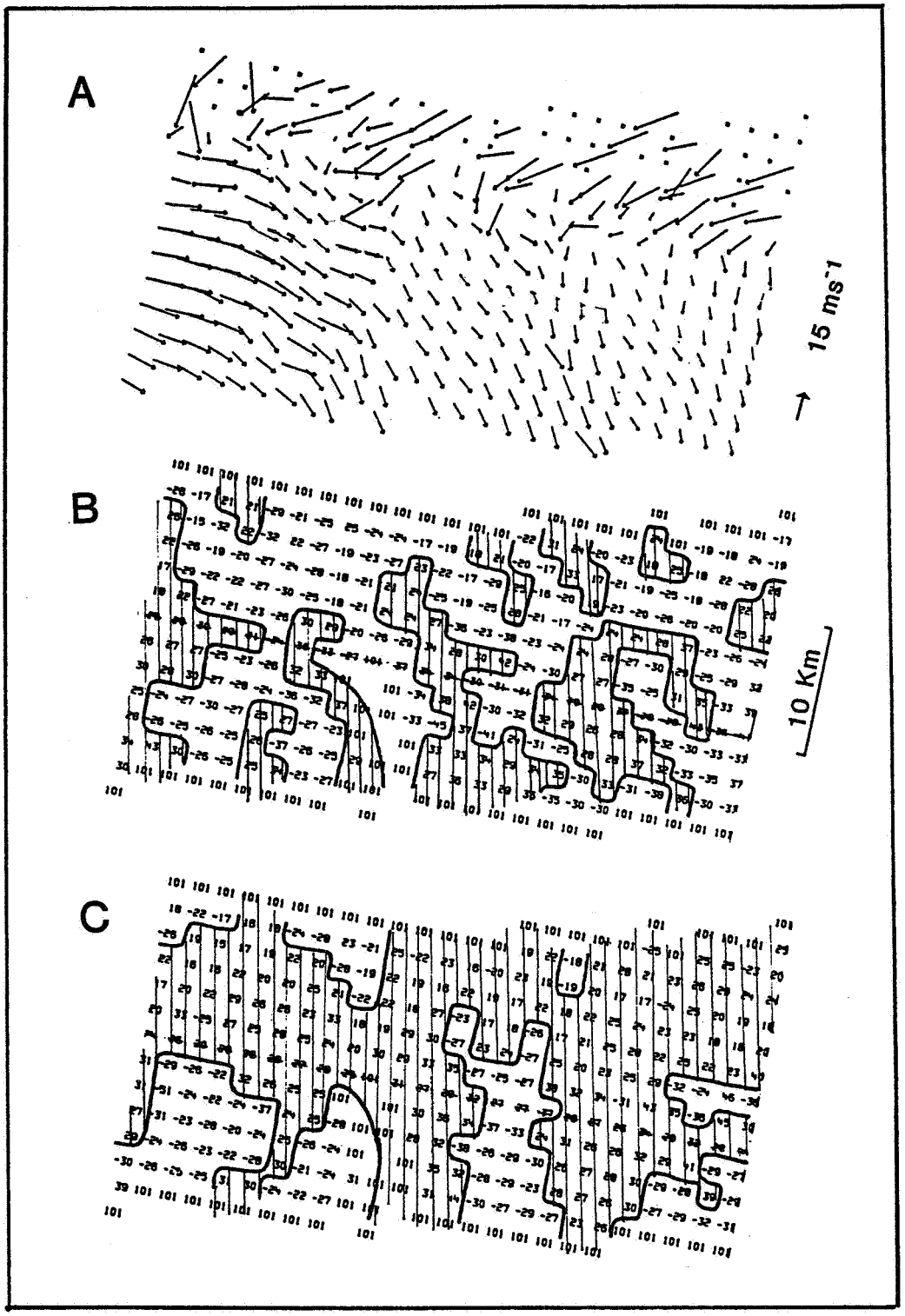

Fig. 17. Airborne Doppler Lidar 1 km averaged wind vectors (17A), divergence (17B), and vorticity fields (17C) for feature A in Figure 16. Temperatures measured onboard the NASA CV990 are presented along the aircraft flight track.

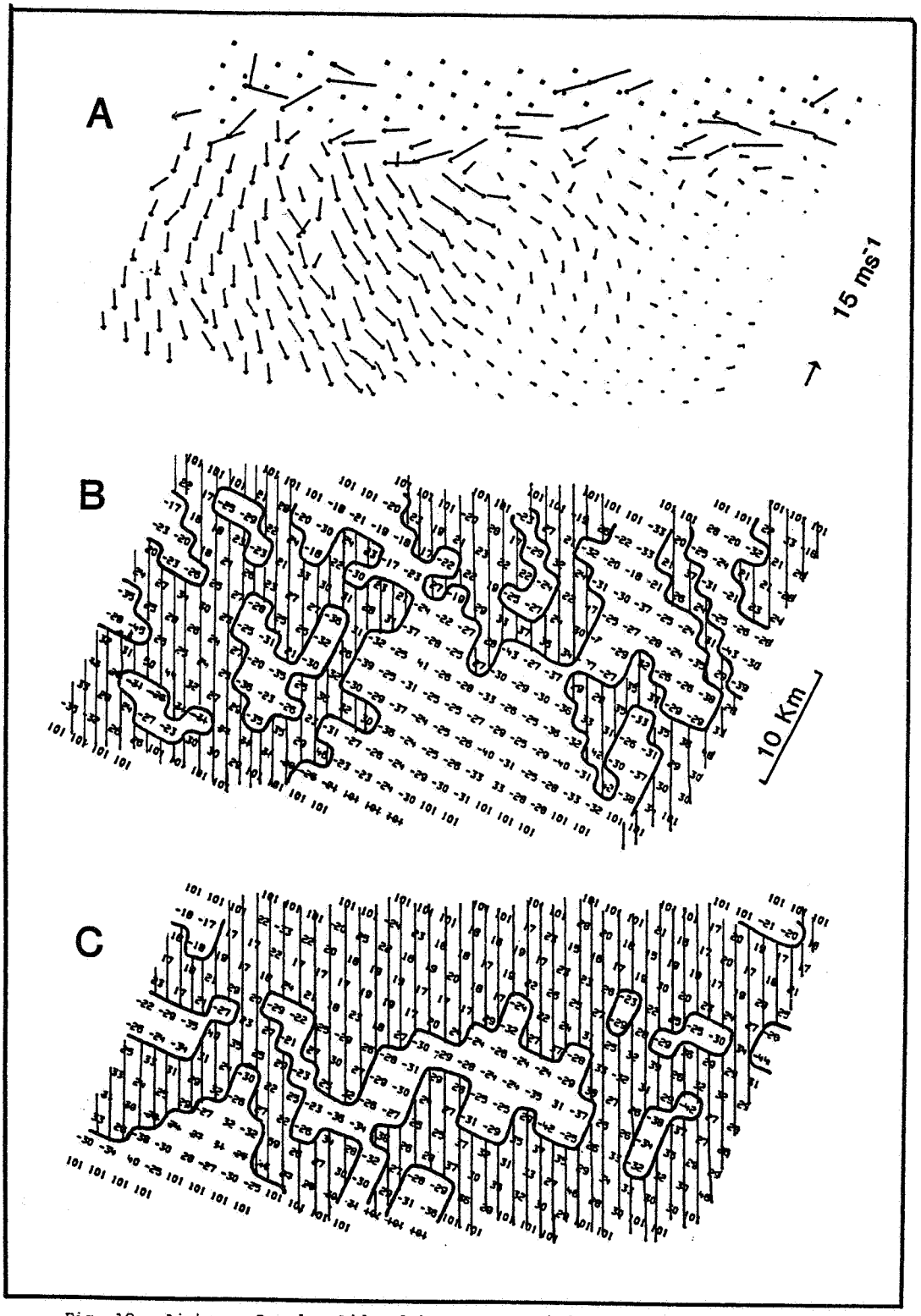

Fig. 18. Airborne Doppler Lidar 1 km average wind vector (18A), divergence (18B), and vorticity fields (18C) for feature B in Figure 16. Temperatures measured onboard the NASA CV990 are presented along the aircraft flight track.

the region above the outflow air--i.e. increased westerly components.

Because the plotted values of divergence and vorticity are not additive, it is difficult to tell at a glance whether these quantities are collectively reasonable. For example, visual inspection of Figures 15 and 17 may suggest that there is significantly more positive vorticity measured on Run 13 along the southern flank of the storm than on Run 12 along the northern flank. Histograms of the vorticity values within 10 km of the flight track are plotted in Figure 19. The net result is that the average vorticity for Run 12 was 1.43×10^{-3} s^{-1}; for Run 13 it was 2.13×10^{-3} s^{-1}--not as large a difference as it may have appeared.

A second pass (Run 14) along the northern flank of the eastward moving storm system was done about 45 minutes after Run 12. In Figure 20 we see a consistent southerly flow with few recognizable convergence zones. After making Run 14 attention was directed toward some growing towers to the north and no further sampling on the main storm was made.

2.2 July 23, 1981

July 23 was a CCOPE-VAS experiment day when five rawinsonde stations in eastern Montana were operated in support of an intensive period of VISSR Atmospheric Sounder (VAS) observations. Due to misprogramming of the scanner on the GOES satellite, the VAS coverage was never far enough north to cover the area in which the storm outflows occured. However, the routine (30 minute) visible and infrared satellite imagery taken during the airborne lidar study period were obtained and considerable effort was made to match satellite and aircraft navigation data. Whereas the outflows on 21 July 1981 were presented primarily to demonstrate the lidar flow visualization capabilities in the boundary layer regions of convective storms, the outflows on 23 July 1981 were examined for possible clues to the merger and evolution of the severe storms that began in SE Montana and propagated into the Dakotas producing heavy rains and large hail.

2.2.1 Synoptic Situation

The surface and 500 mb maps for 1200 Z 23 July 1981 and 0000 Z 24 July 1981 are shown in Figures 21 and 22. During the period of airborne lidar observations (2200-2300 Z) a cold front had pushed to within a 200 km of the storm on the Montana-South Dakota (M/SD) boundary. The surface winds in the undisturbed region east of the front were easterly around 10-15 kts.

2.2.2 Storm Characteristics

A. Radar time histories

The early phases of the M/SD storm occurred just within range of the Skywater surveillance radar (Figure 23). However, at the time the CV990 was flying the outflow mission (2200-2300 Z) the storm was just moving out of radar range so that only the north-western part

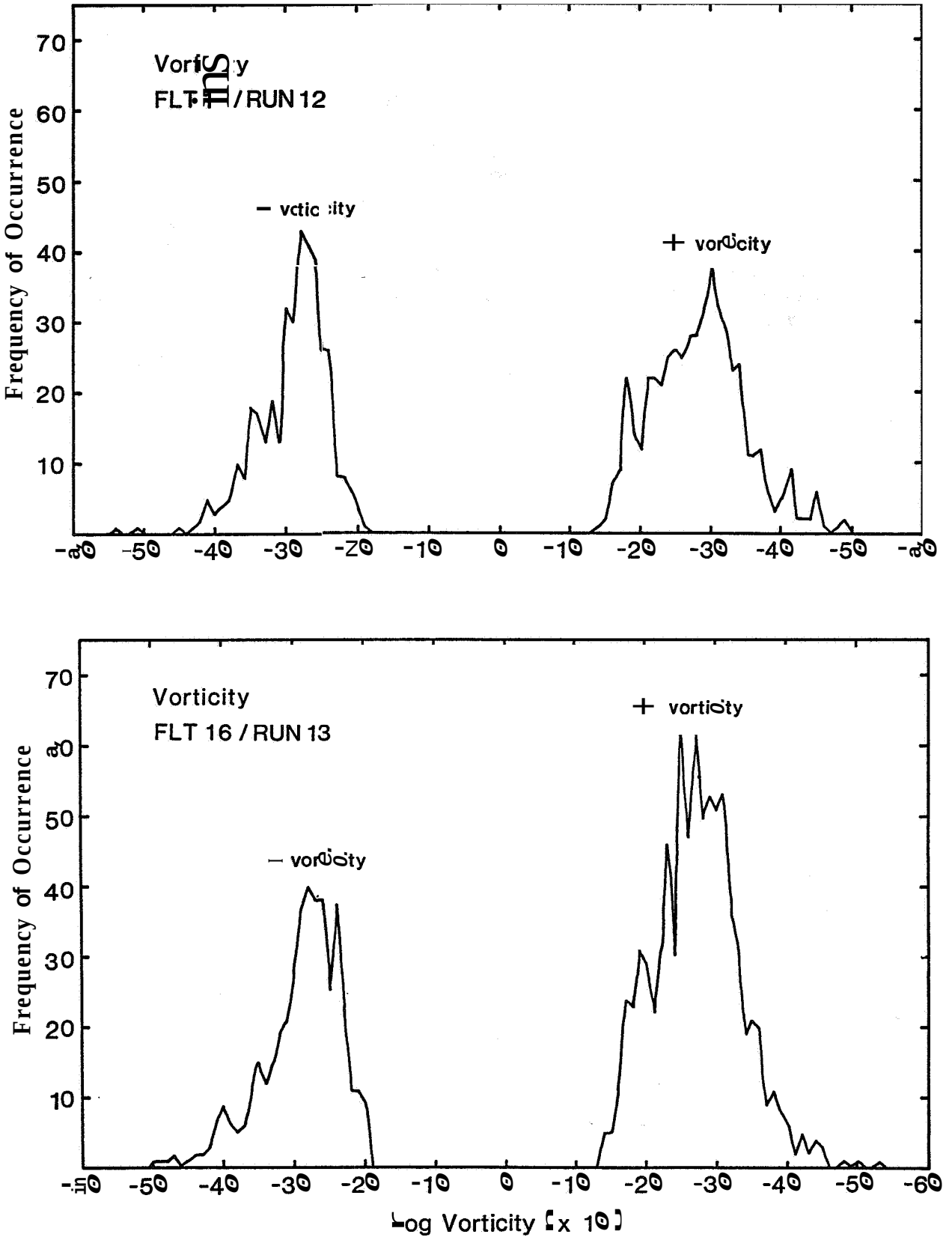

Fig. 9 Histograms of vorticity values taken from the 1 km averaged ADL wind fields for Flight 16 runs 12 and 13.

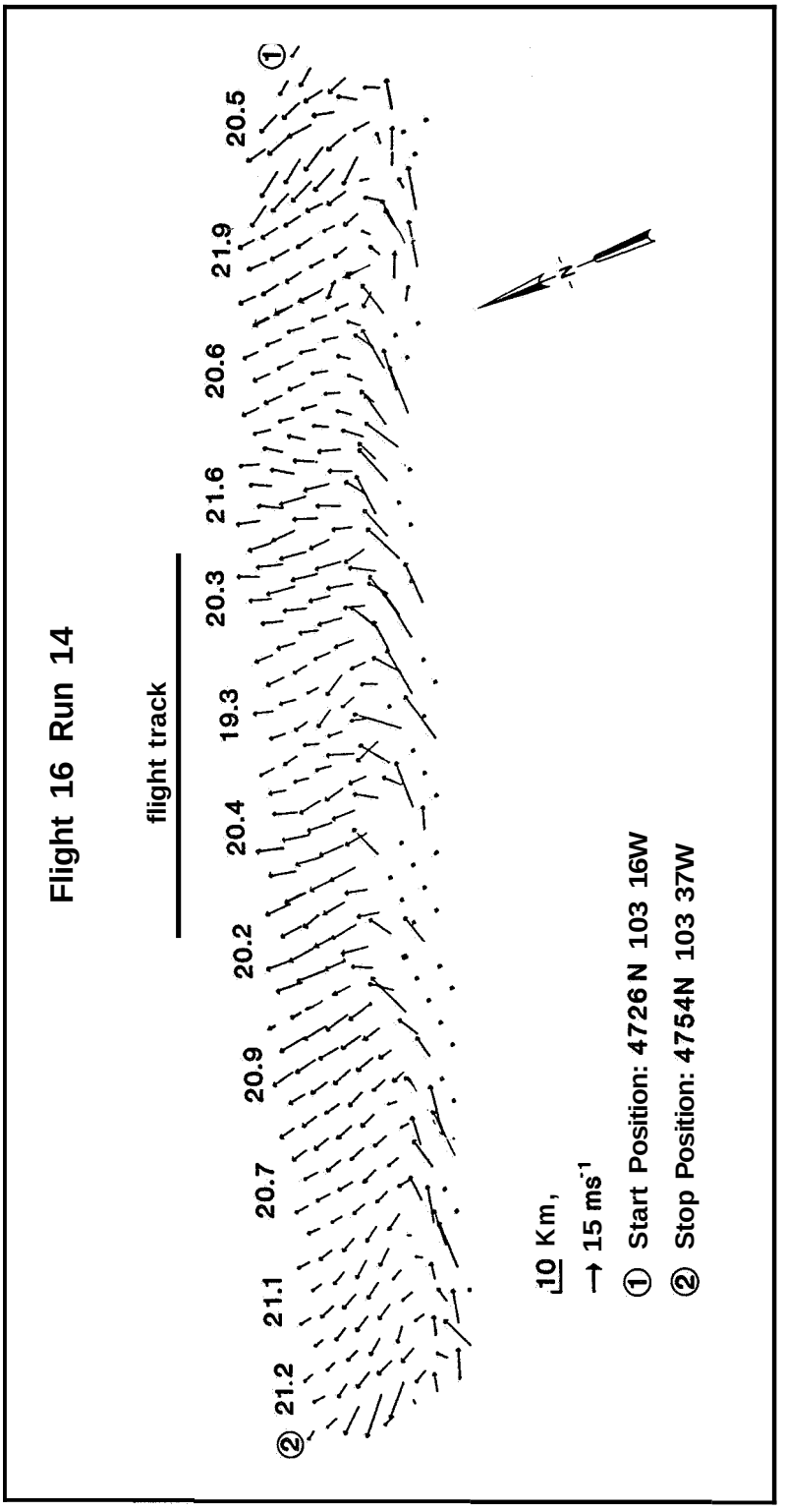

Fig. 20. Airborne Doppler Lidar winds obtained during Flight 16 run 14 (0009 - 0019 Z) 22 July 1981. Wind vectors represent 2 km dverages of the full resolution (330 m) wind data. Temperatures measured onboard the NASA CV990 are presented along the aircraft flight track.

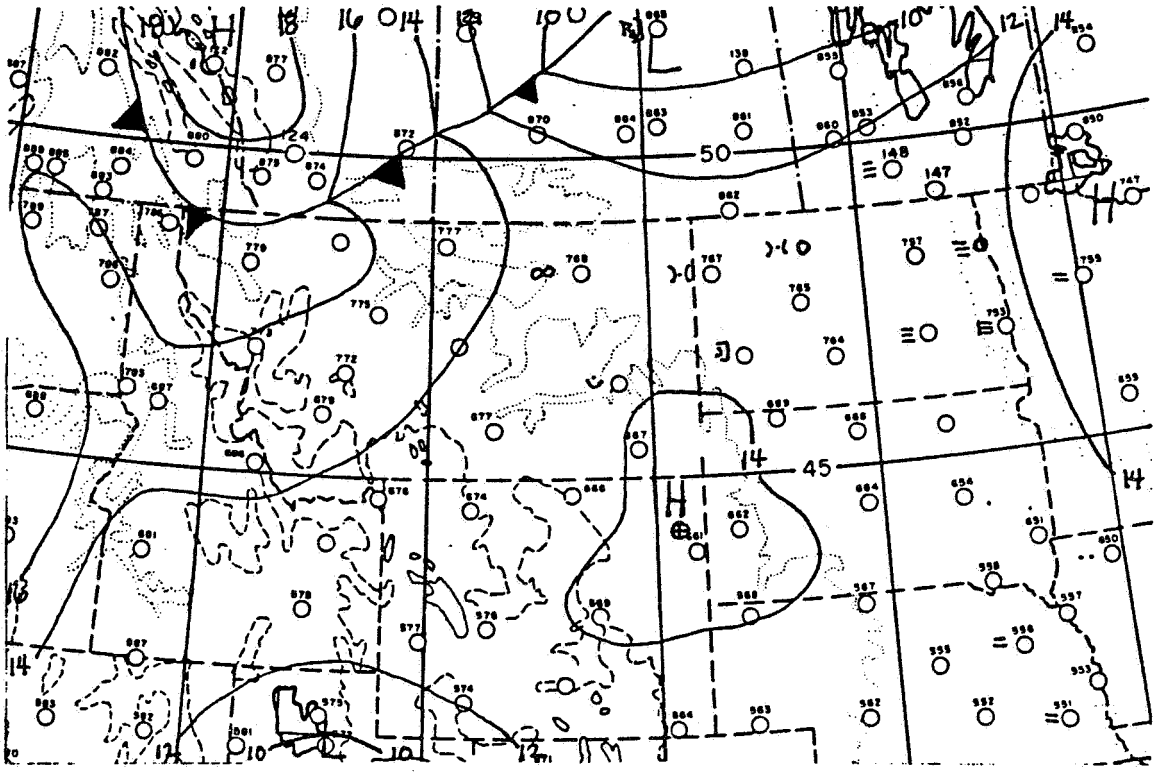

Fig. 21. A. Surface Map Analysis and Weather for 1200 GMT 23 July 1981.

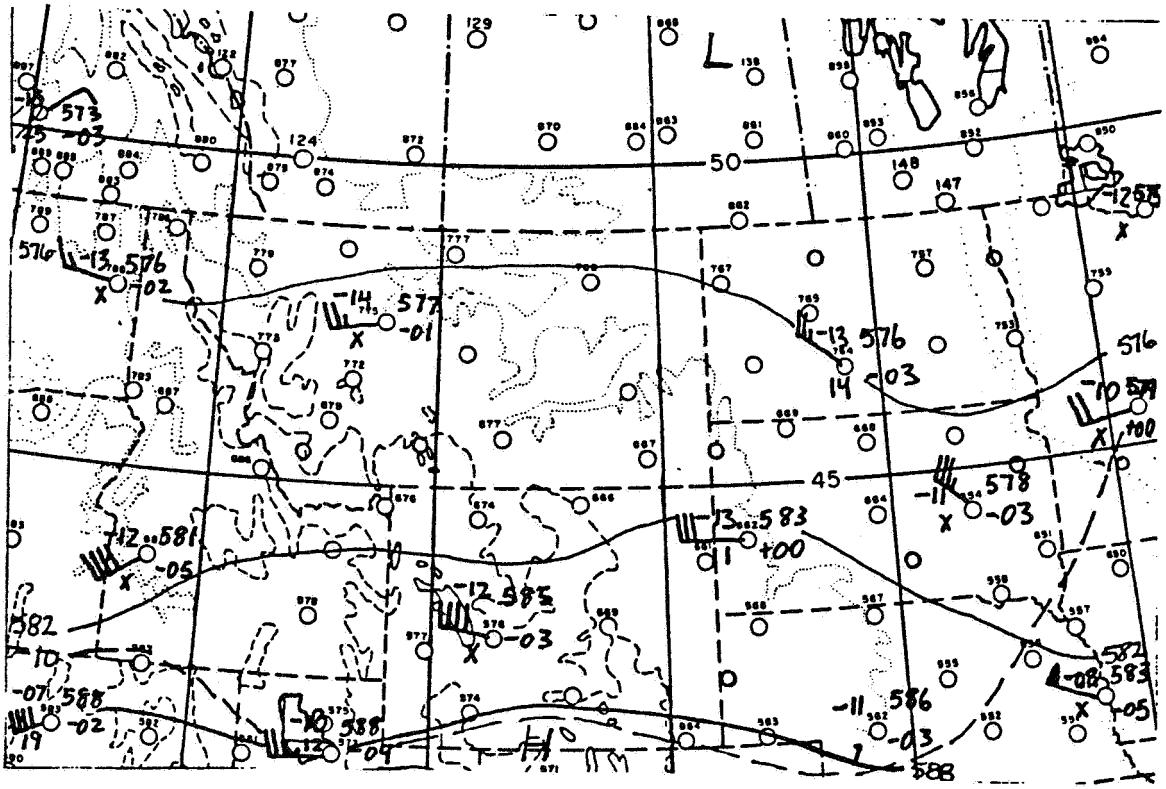

B 500 mb Map for 1200 GMT 23 July 1981

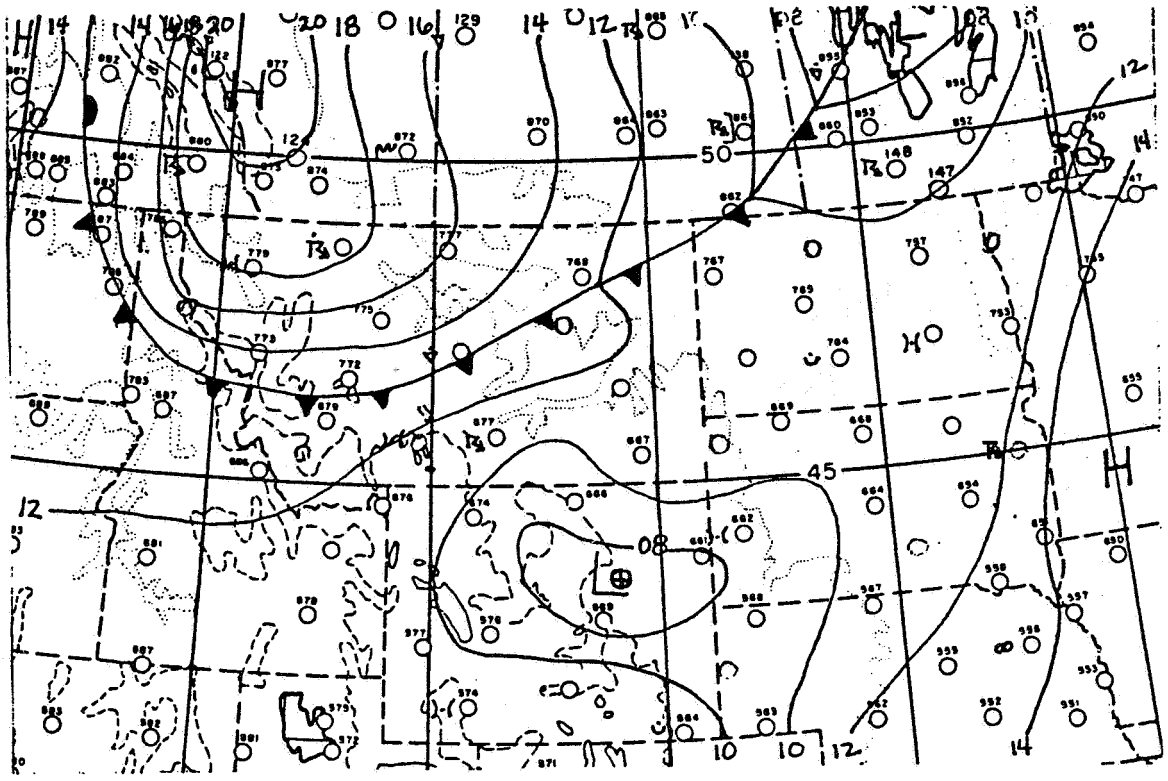

Fig. 22 A. Surface Map Analysis and Weather for 0000 GMT 24 July 1981.

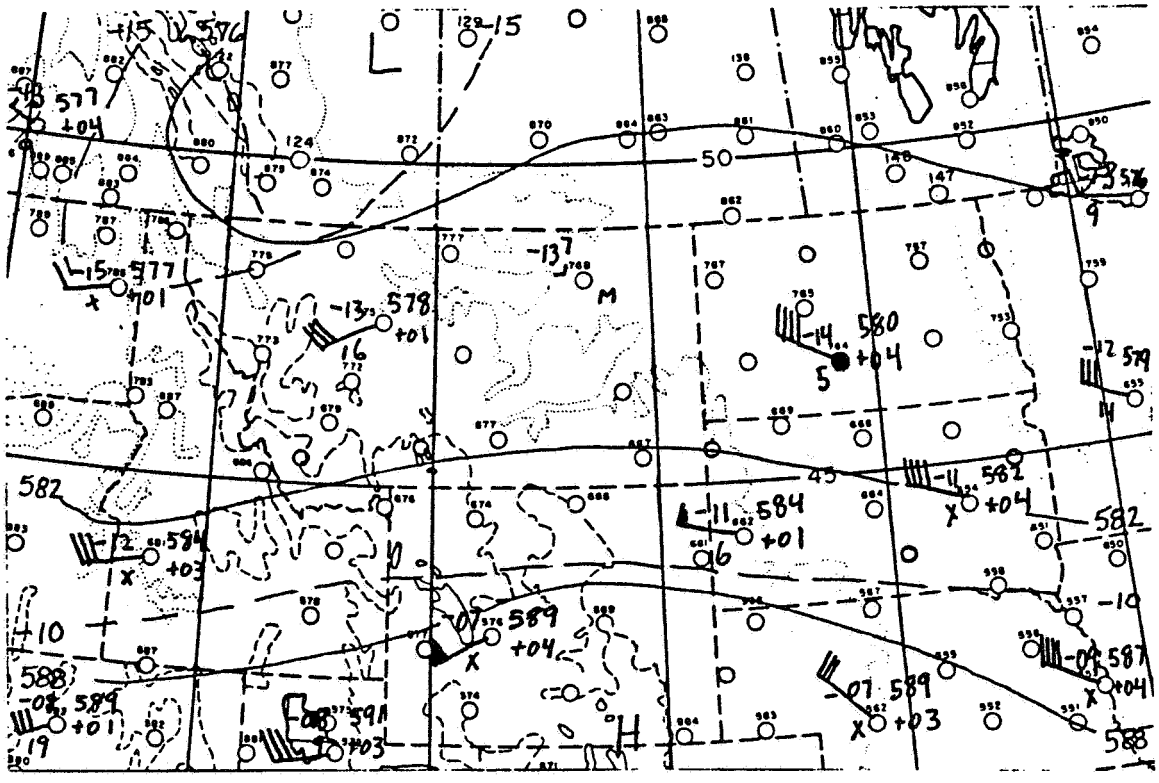

B. 500 mb Map for 0000 GMT 24 July 1981.

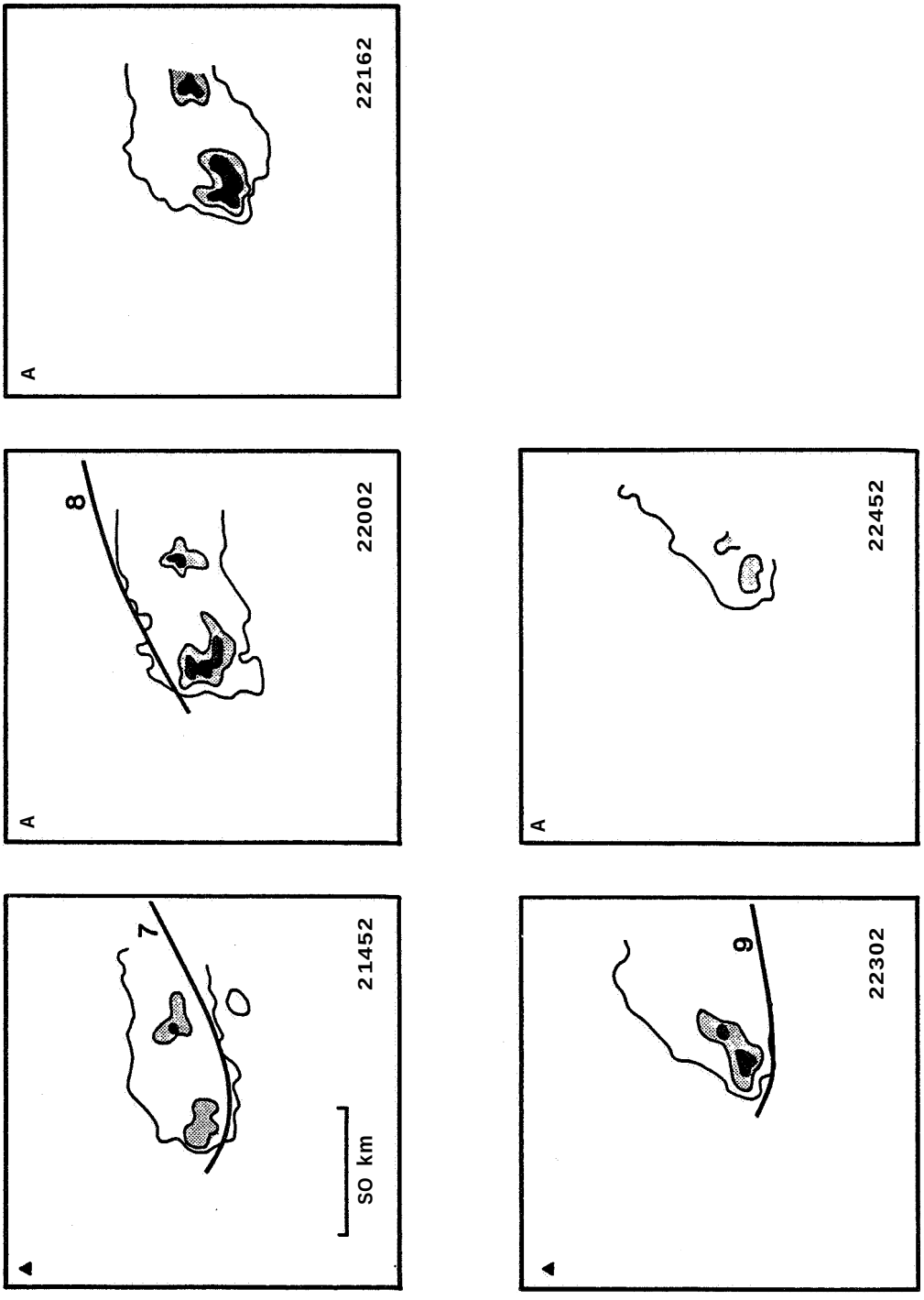

Fig. 23. 23 July 1981 radar echo time history for the 30, 40 and $\geq$ 50 dbz contours. CV990 Flight 17 paths are superimposed for runs 7, 8 and 9.

of the complex was being detected. The 2230 Z radar echo map was used as an overlay on the satellite imagery. At this time 50-60 dbz returns were recorded by ground radar while airborne observers commented on "separate beautiful clouds" growing side-by-side. The second cloud complex was just to the southeast of the one being sensed by the SWR-75.

B- Surface Network Observations

Unfortunately the storm being studied by the airborne lidar moved beyond the eastern boundaries of the surface network (Figure 24). However, the surface data showed evidence that, contrary to the synoptic analysis, the cold front may have passed through the CCOPE area prior to 0000 Z. Note in Figure 25 that the wind shift from southeasterly to northerly and moderate temperature drops of 2 - 5°C progressed from the NW to the SE as would be expected with a frontal passage. In the extreme SE corner of the CCOPE area, further temperature drops of up to 9°C (2200 Z) were recorded during the time that the CV990 was on runs 7 and 8 (Figure 26).

C- Satellite Imagery

The evolution of the Montana/South Dakota storm as seen in the satellite visible imagery is presented in Figures 27 to 33. The focus of the airborne observation was on the "B" portion of the storm complex with special interest in the bridge clouds that formed around 2230. After the airborne lidar mission period the "A" and "B" developments merged and moved eastward with further development on the S-SW edge of the complex.

D Airborne Doppler Lidar System

At 2213 the CV990 began a NE-SW run down the northern flank of the "B" portion of the storm. The lidar was scanning underneath a rather continuous cloud mass punctuated with rain showers. At 2230 the aircraft turned back to an easterly heading that took it right between the two towering developments. To provide the general sense of the wind field as detected by the airborne lidar, the 330 m wind vectors were averaged to 2 km resolution and overlayed on the visible cloud imagery (2230) and, to the extent available, the Skywater radar echo map (Figure 34). The length of the arrows in Figure 34 are all equal; only the direction is to be taken as information. Several features in that figure need to be highlighted, starting in the upper right and moving counterclockwise:

1) the undisturbed flow is from the east, suggesting that this convection was just ahead of or above the cold front,

2) near the areas of strong radar echo returns the winds show deflection consistent with rain shaft divergent outflows,

3) the small cloud along the left border of the figure is part of an "arc" of clouds that can best be seen on a film loop of satellite imagery between 2200 and 2400 GMT, and

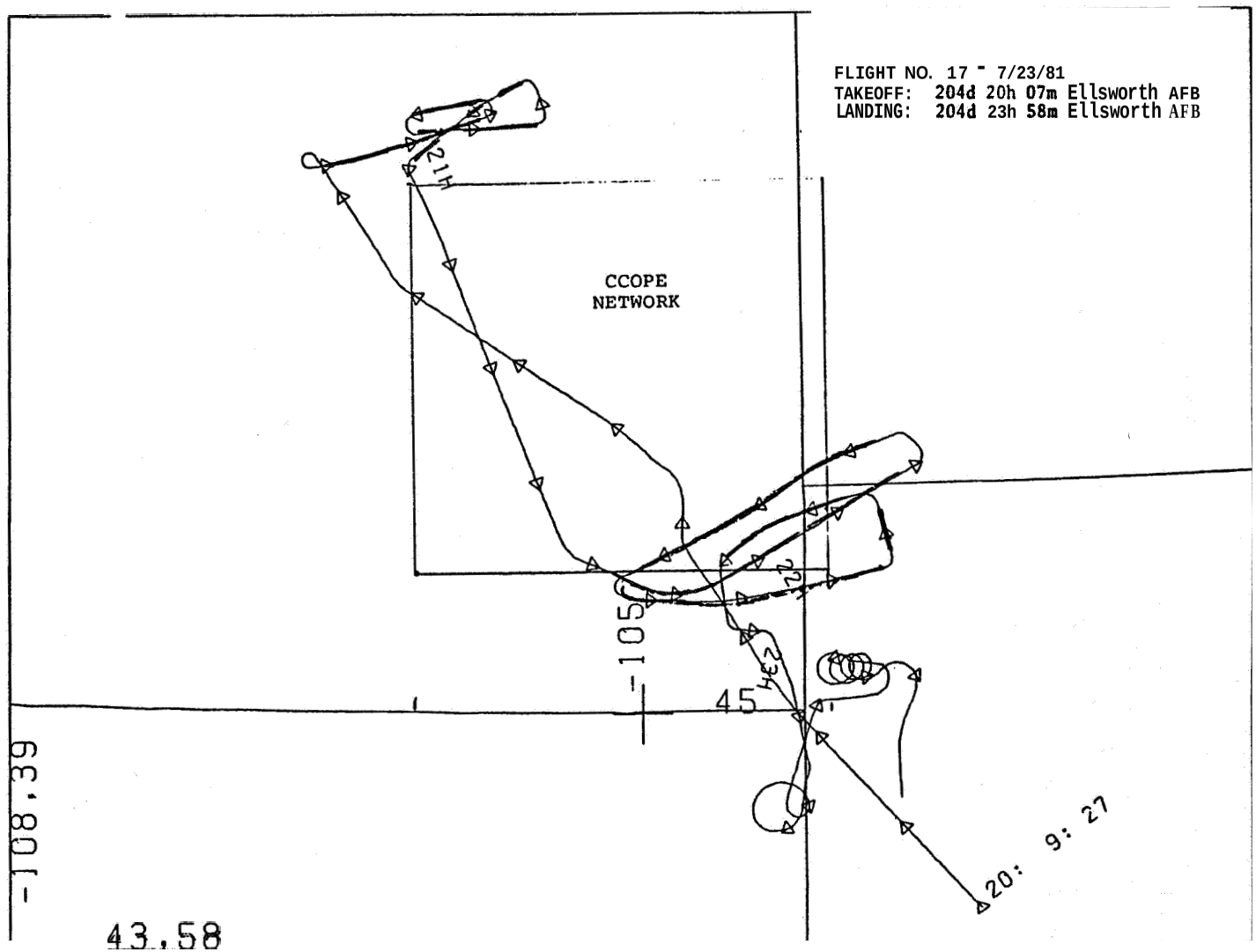

Fig. 24. Flight 17 CV990 flight tracks on 23 July 1981. Darkened portions of the track were in the vicinity of the target storm. The boundaries of the CCOPE surface network are shown as well as the nearby state boundaries.

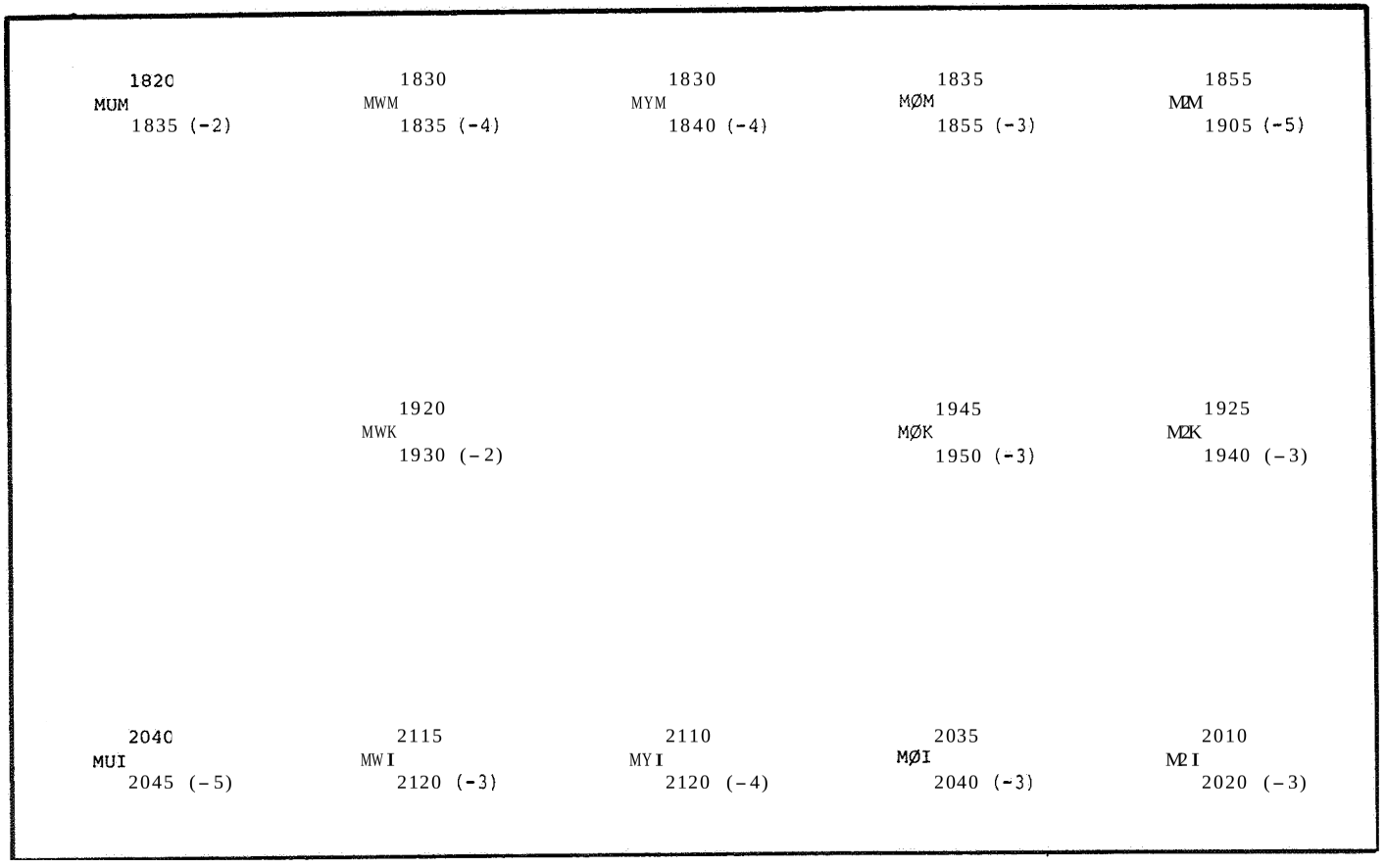

Fig. 25. **Southeast section of** CCOPE **surface network with times (noted above surface station identification) of wind shift from southeasterly to northerly and times (noted below surface station identification) Of first major temperature drop (≥ 2°C). Number in parentheses is the magnitude of the temperature drop.**

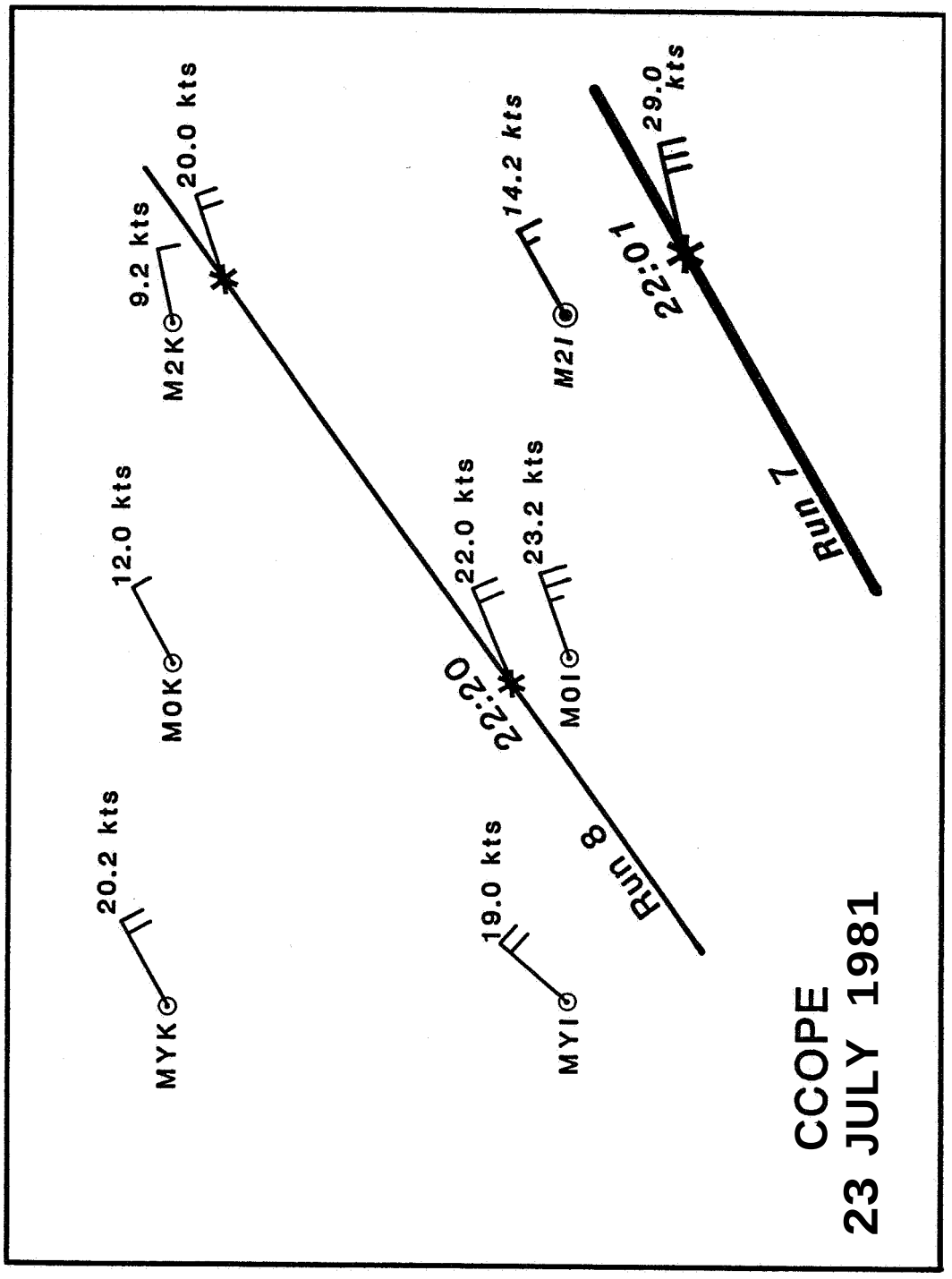

Fig. 26. Section of CCOPE surface network over which the CV990 flew during runs 7 and 8 of Flight 17 on 23 July 1981. Wind flags on the aircraft track are shown for times of closest approach to a surface station by the aircraft flying at 400 m AGL. Times (GMT) are noted above the flight track while the INS winds are noted with a wind flag.

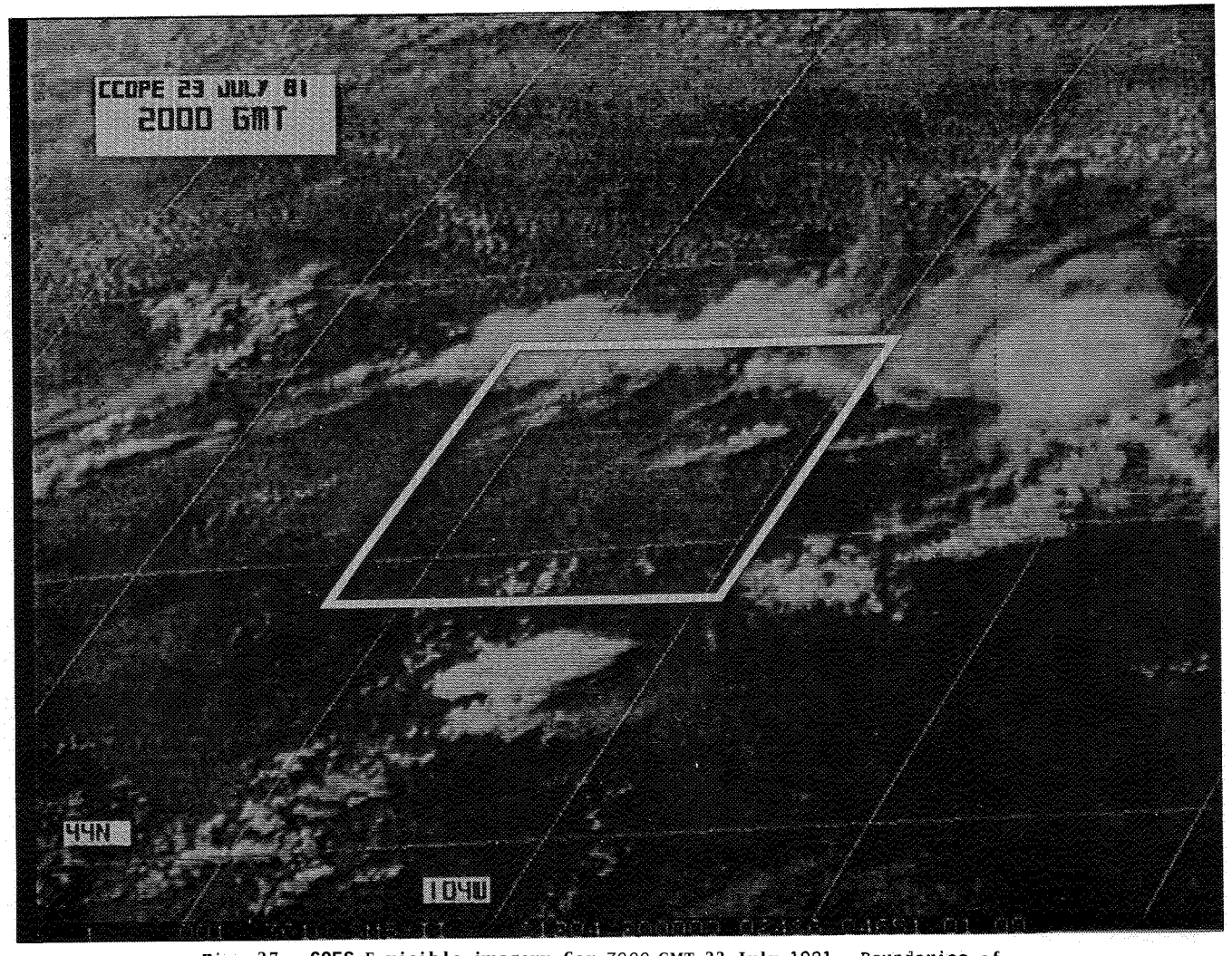

Fig. 27. GOES E visible imagery for 7000 GMT 23 July 1981. Boundaries of CCOPE surface network are provided for reference. Latitude and longitude lines are at 2° spacing.

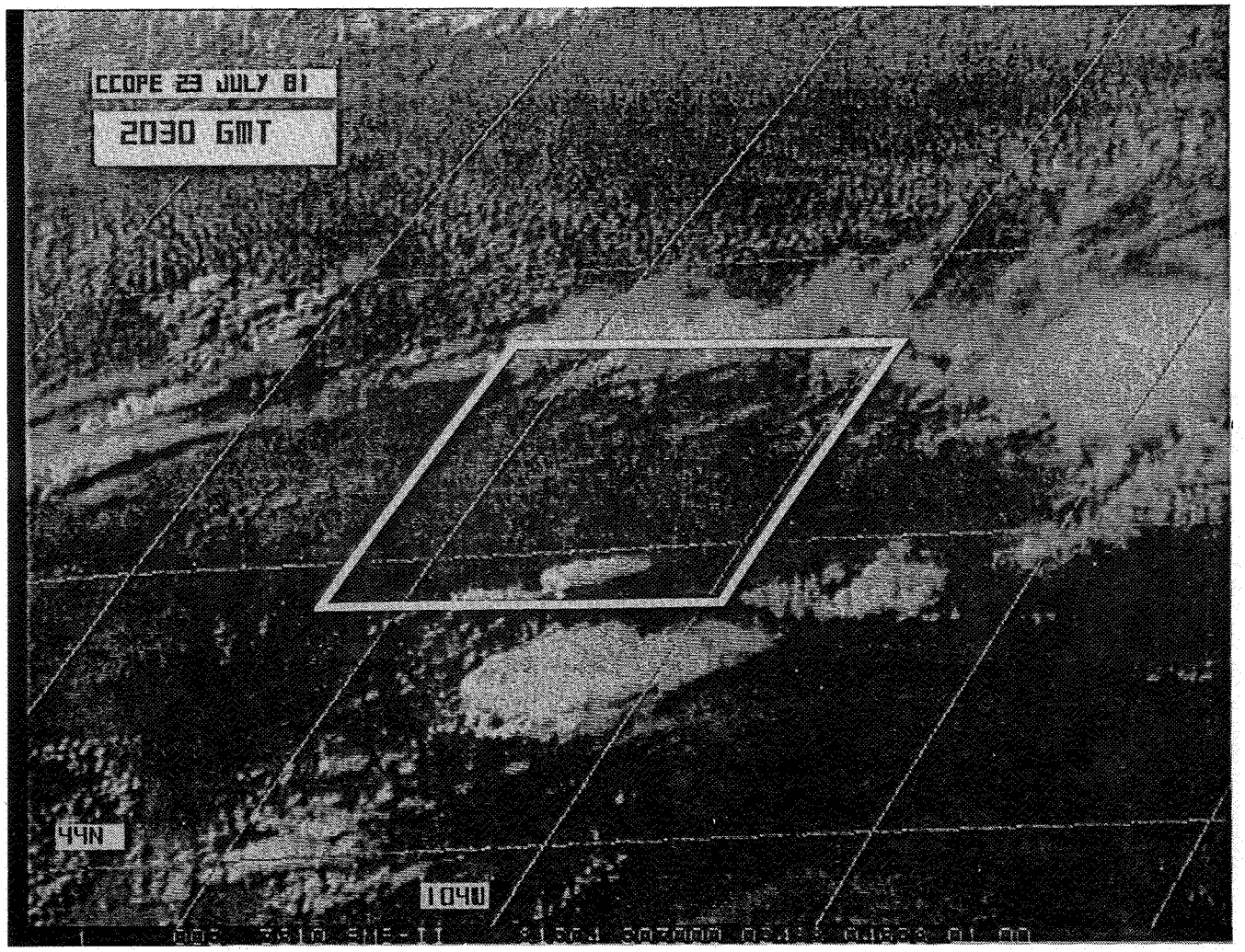

Fiq. 28. GOES E visible imagery for 2030 GMT 23 July 1981. Boundaries of CCOPE surface network are provided for reference. Latitude and longitude lines are at 2° spacinq.

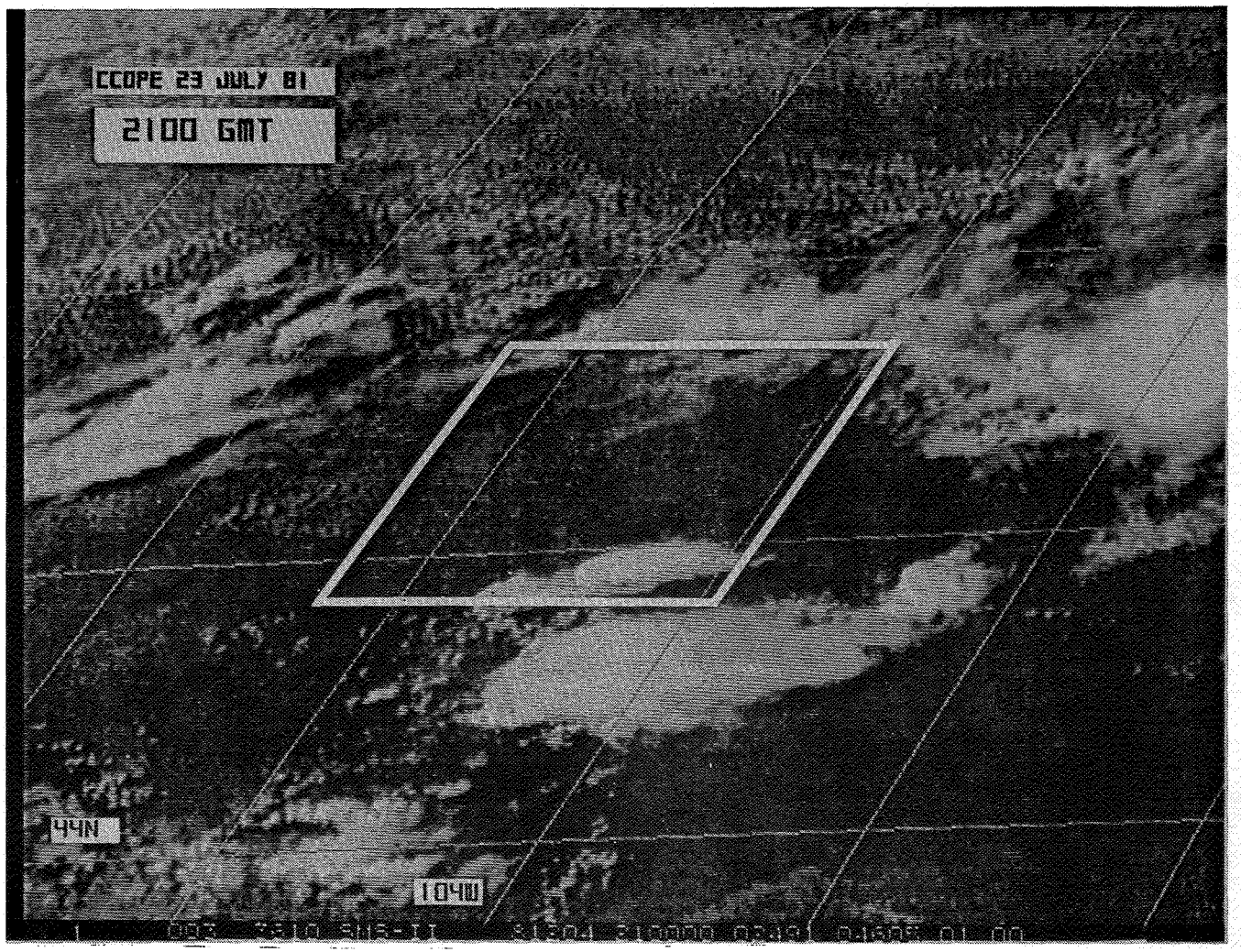

Fig. 29. GOES E visible imagery for 2100 GMT 23 July 1981. Boundaries of CCOPE surface network are provided for reference. Latitude and longitude lines are at 2^{o} spacing.

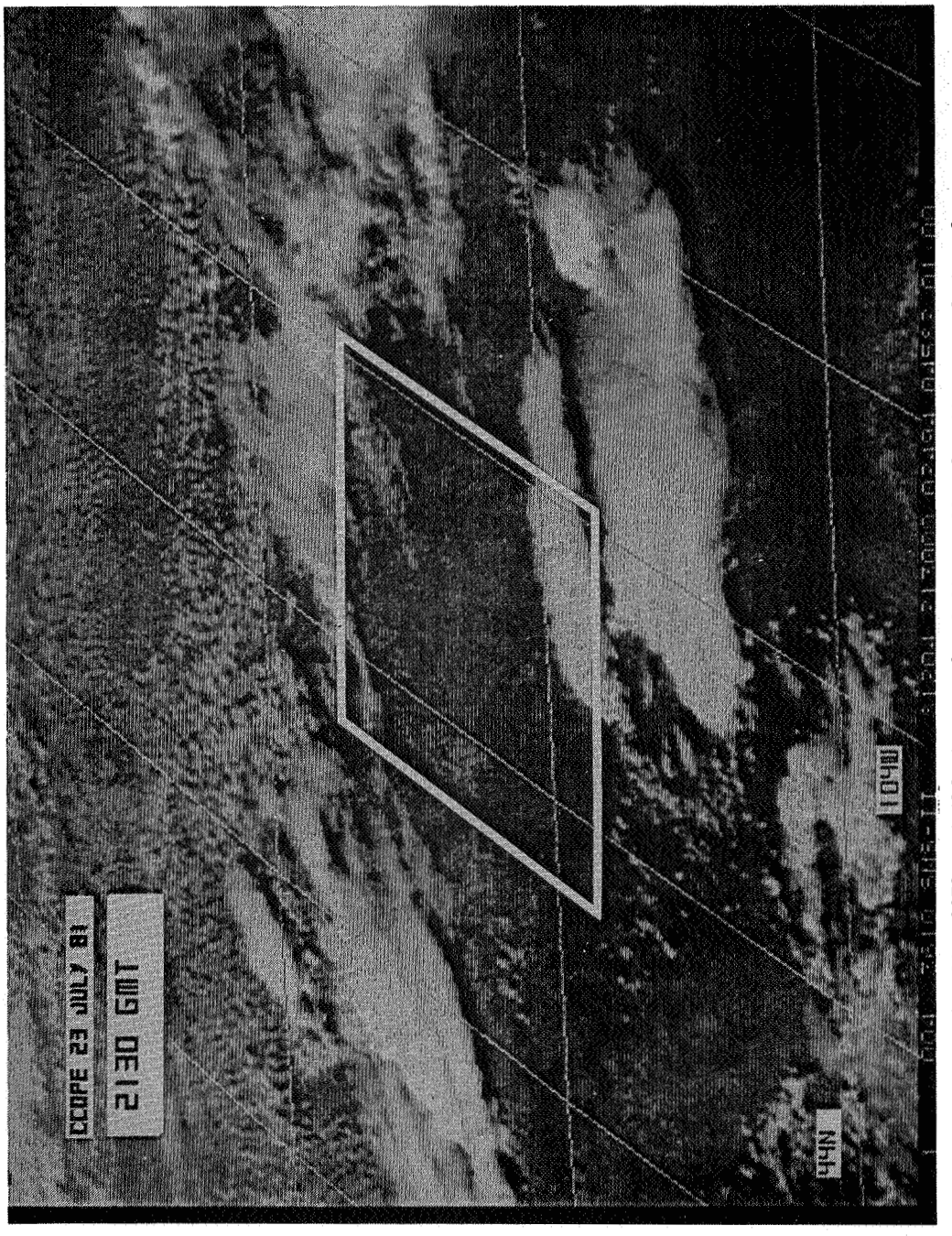

Fig. 30. GOES E visible imagery for 2130 GMT 23 July 1981. Boundaries of CCOPE surface network are provided for reference. Latitude and longitude lines are at 2° spacing.

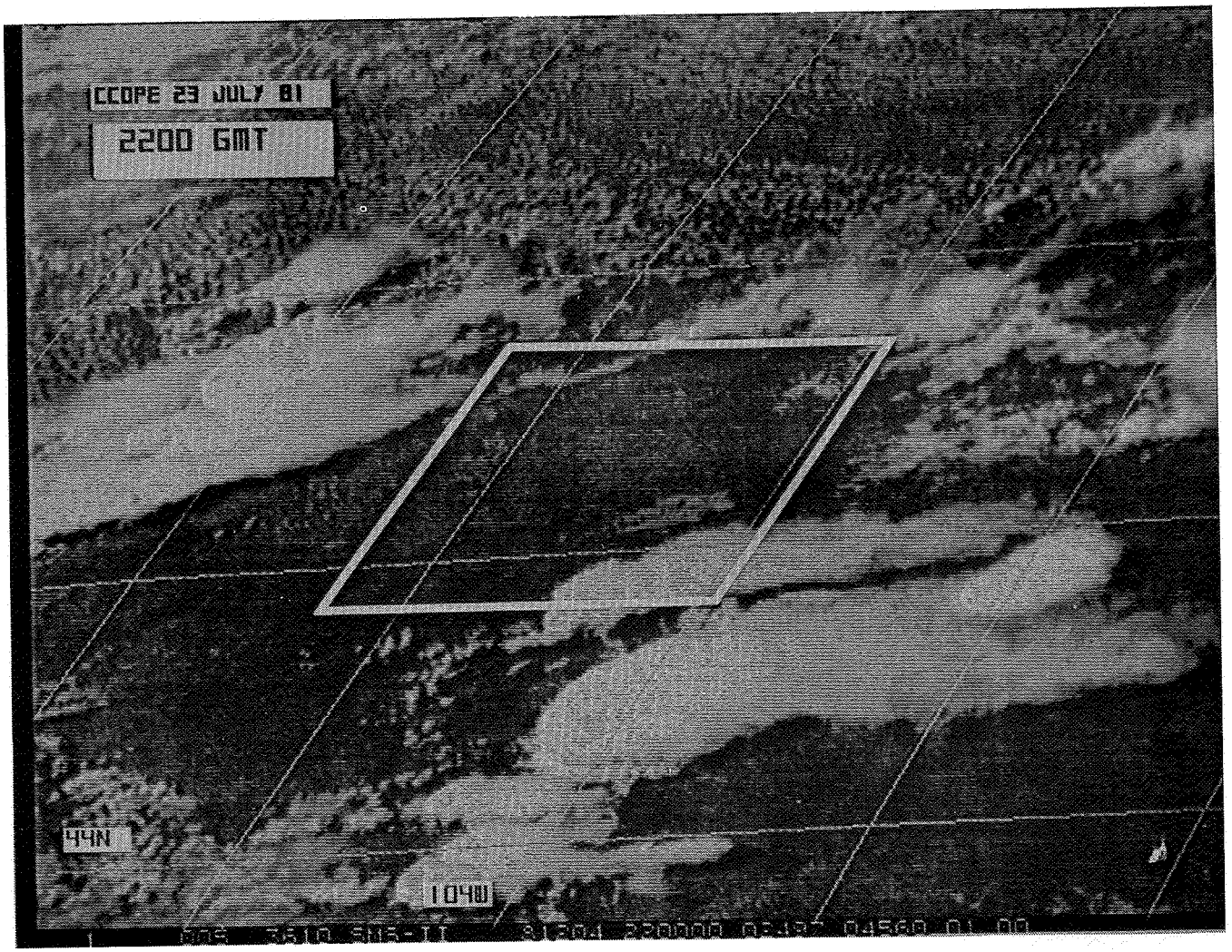

Fig. 31. GOES E visible imagery for 2200 GMT 23 July 1981. Boundaries of CCOPE surface network arc provided for reference. Latitude and lonqitude lines are at 2^{O} spacing.

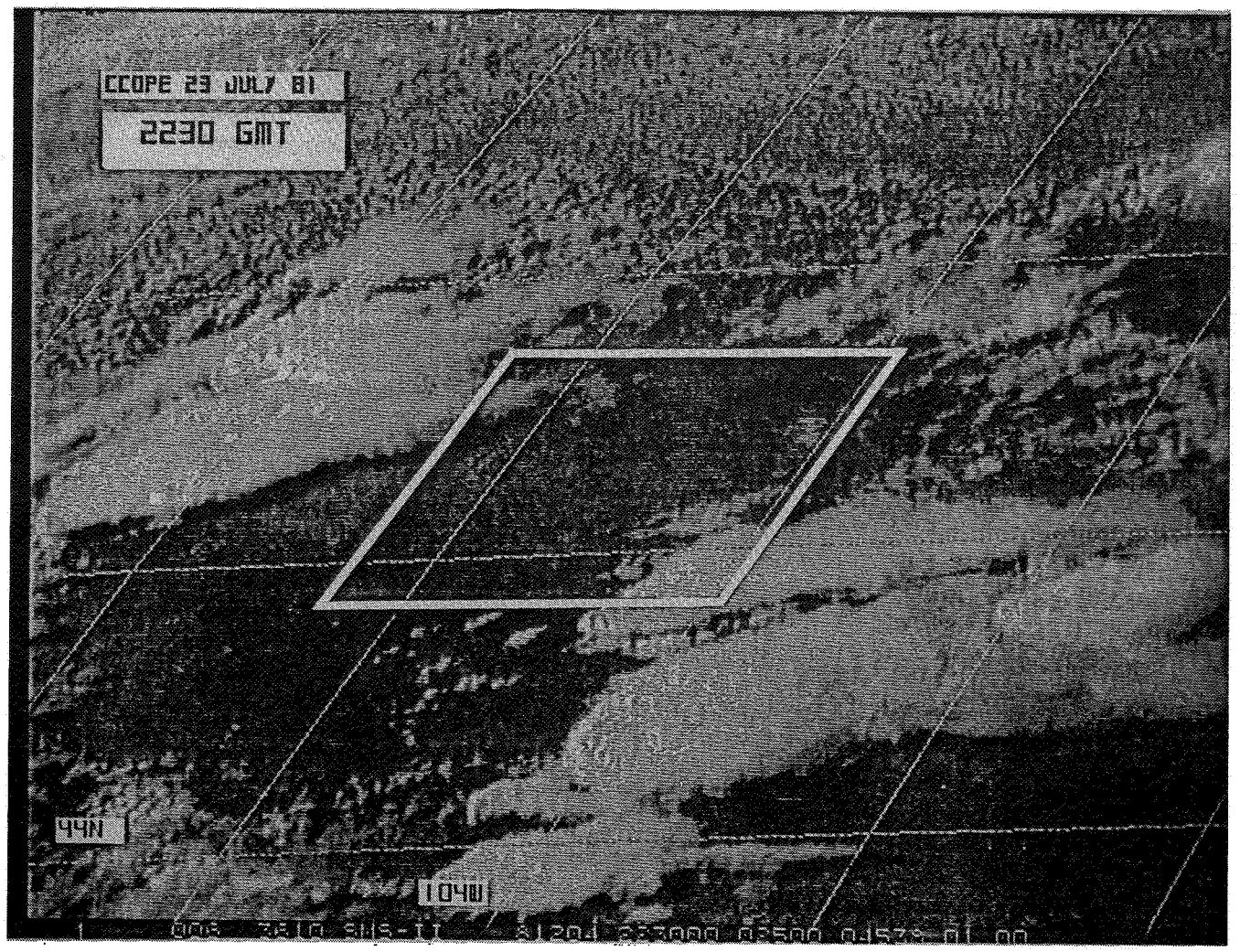

Fiq. 32. GOES E visible imaqery for 2230 GMT 23 July 1981. Boundaries *of* CCOPE surface network are provided for rcfercnce. Latitude and lonqitude lines are at 2° spacing.

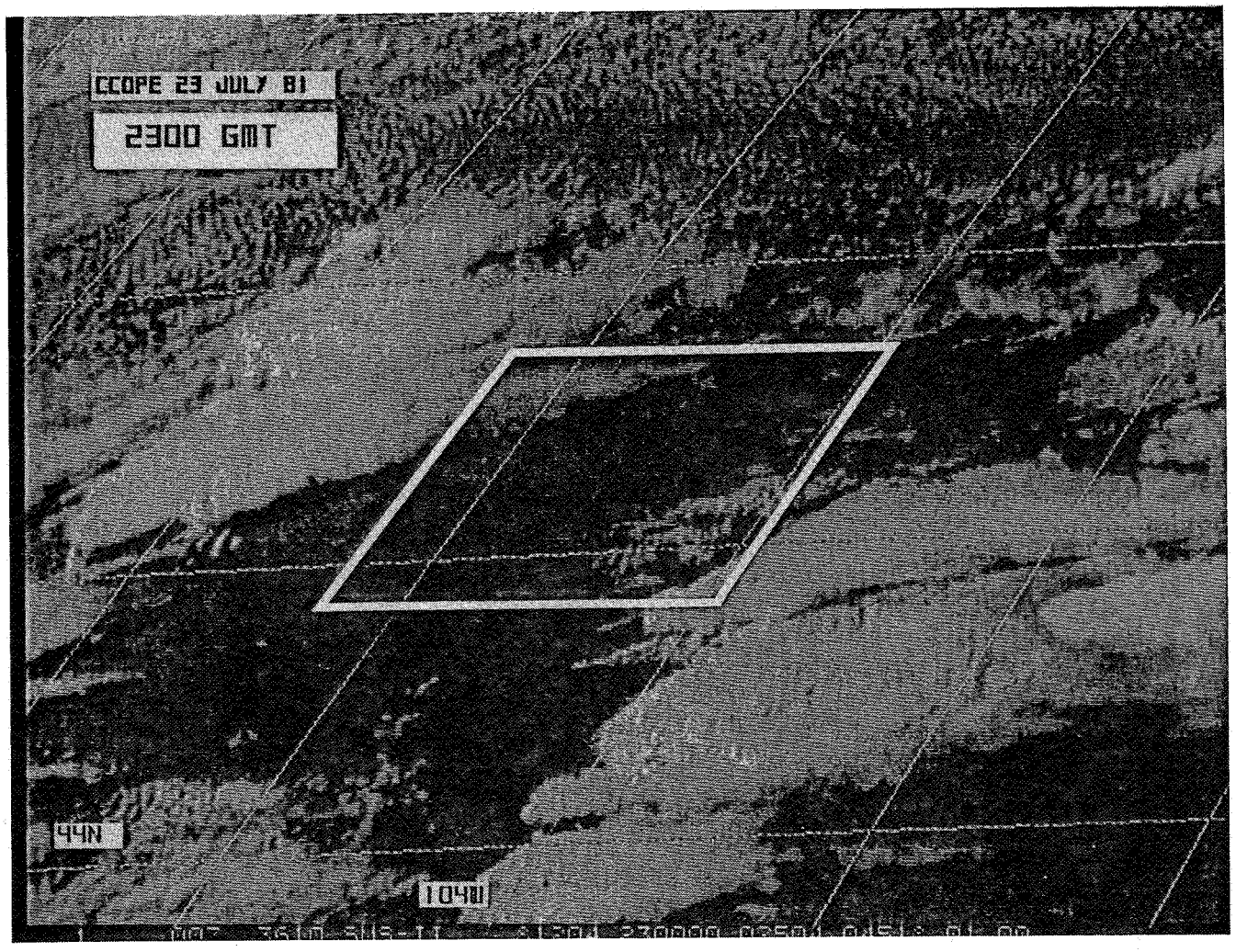

Fig. 33. GOES E visible imagery for 2300 GMT 23 July 1981. Boundaries of CCOPE surface network are provided for reference. Latitude and longitude lines are at 2° spacing.

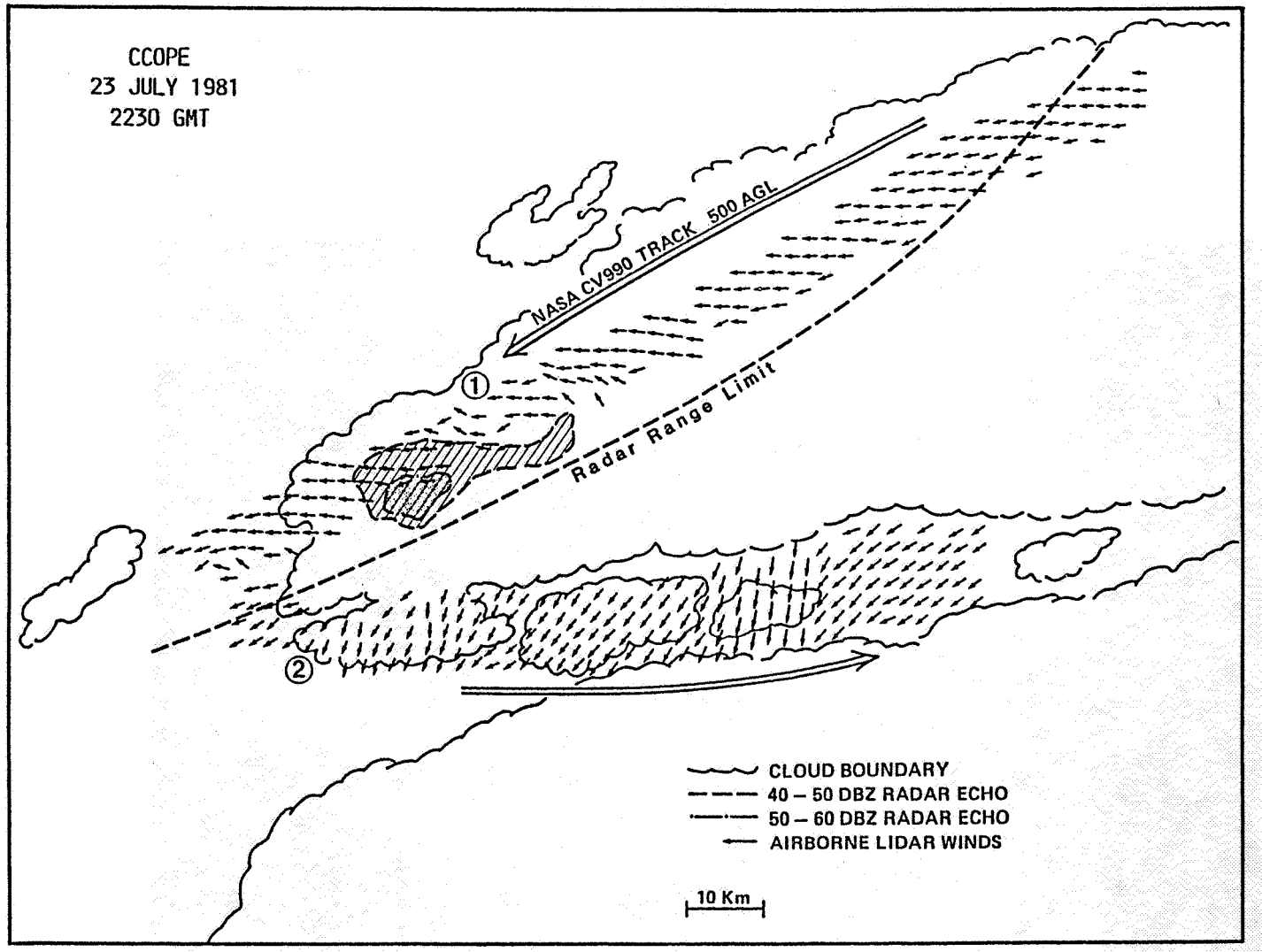

Fig. 34. Overlay of ADL wind vectors on the cloud boundaries as seen on satellite imagery and the >40 DBZ radar echoes as measured by the SWR-75 radar. The lengths of the wind vectors are all equal--only directional information is available from this figure. Flight altitude is 500 m AGL.

4) on the easterly track, strong outflow from the north was encountered and as shown seemed to be limited to the region where new convection was being detected by satellite. The strength of this outflow was ~35-45 knots.

The divergence and vorticity fields calculated from the 2 km resolution lidar wind fields are presented in Figures 35 and 36. It is difficult to say much about these calculated quantities except that they are coherent on scales of 10-20 km and are of reasonable magnitude ($\sim 10^{-4}$ - 10^{-3} s^{-1}) for convective areas.

Much more detail is available with the 330 m resolution lidar wind data. Regions noted as "1" and "2" in Figure 34 are blown up to full resolution in Figures 37 and 38.

From the satellite imagery we note that around 2230 Z a line of new cells was forming between the two major storms. With the ADLS, a very strong (~40 kts) outflow from the northern complex was detected directly underneath these new cells. Subsequent satellite imagery documents a merger of the two storms and the evolution into a much larger system. Without temperature and vertical velocity information it is left to conjecture that the outflows were responsible for the line of "bridge" clouds which appeared to participate in the development of a more extensive storm entity.

SUMMARY

Wind data obtained with the NASA/MSFC's Airborne Doppler Lidar System during the CCOPE (1981) have provided several examples of the two-dimensional nature of vector and scalar fields in the sub-cloud layer near deep-precipitative convection. The ADLS has demonstrated its unqiue ability to be flown to an area of interest and to obtain a 10-15 km wide map of the horizontal wind field with 330 m spatial resolution. The accuracy of the ADLS measurements remains difficult to assess due to the non-conventional manner in which the winds are obtained. However, there has been good (or reasonable) agreement on every occasion that a comparison could be made with surface anemometer, aircraft INS winds or rawinsonde winds.

On the two days (21 and 23 July 1981) during the CCOPE period, the ADLS "storm outflow" observations lead to the following conclusions regarding the ADLS performance as well as the atmospheric phenomena encountered:

1) the ADLS can be easily navigated near and in highly convective regions to obtain data for severe subcloud layer storm features;

2) the useful range of the two-dimensional wind field measurements is between 10 and 15 km to the left of the aircraft track;

3) the coherence between neighboring (but totally independent) wind vector, divergence and vorticity measurements is reason for relying on the ADLS products to describe kinematic features with length scales near 700 m;

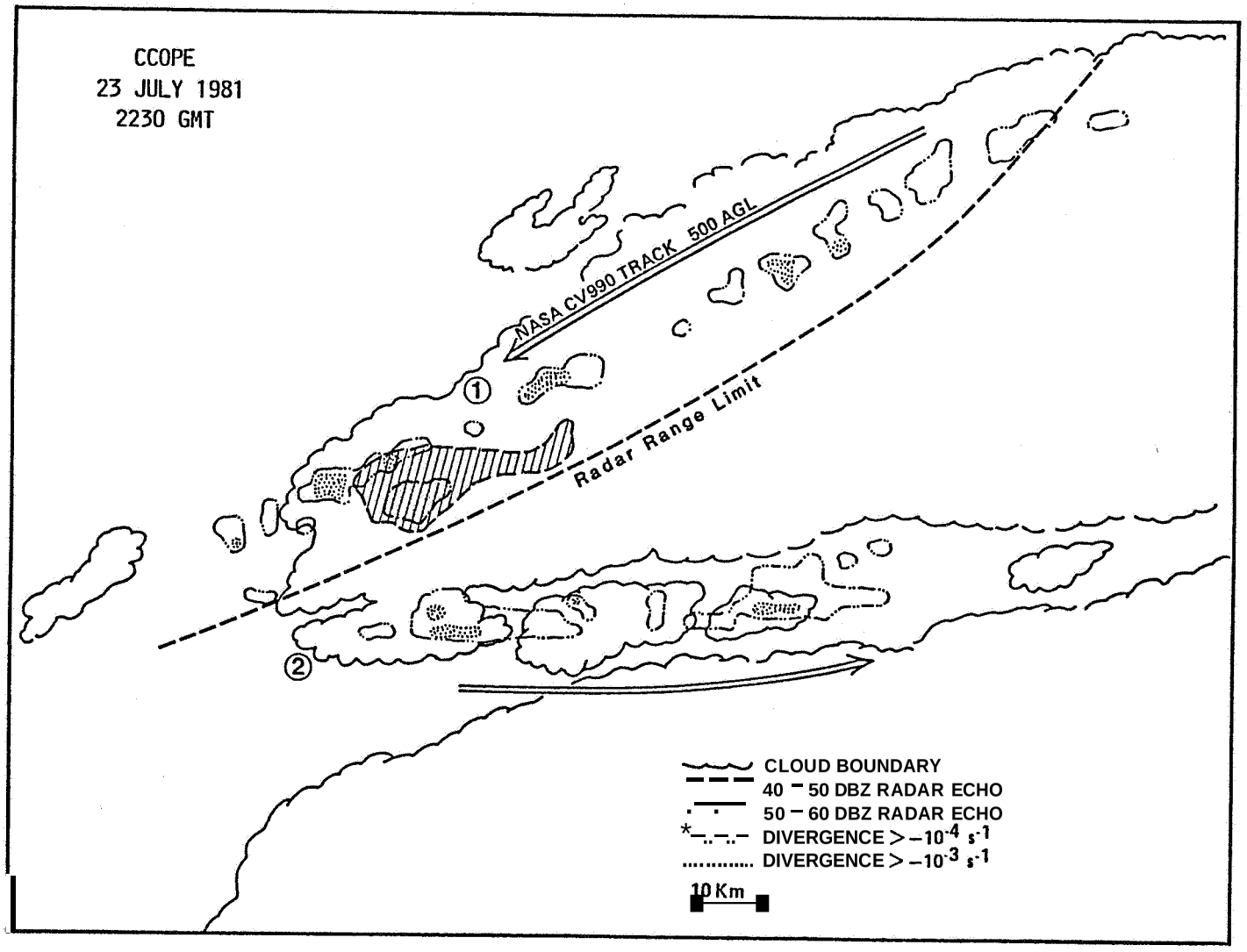

Fig. 35. Overlay of ADL wind divergence field on the satellite derived cloud boundaries and the SWR-75 radar echo map. DIVERGENCE > -10^{-4} s^{-1} includes any values between -10^{-4} and 0 s^{-1}; >-10^{-3} s^{-1} includes any values between -10^{-3} and 0 s^{-1}--i.e. only zones of convergence are plotted. Flight altitude is 500 m AGL.

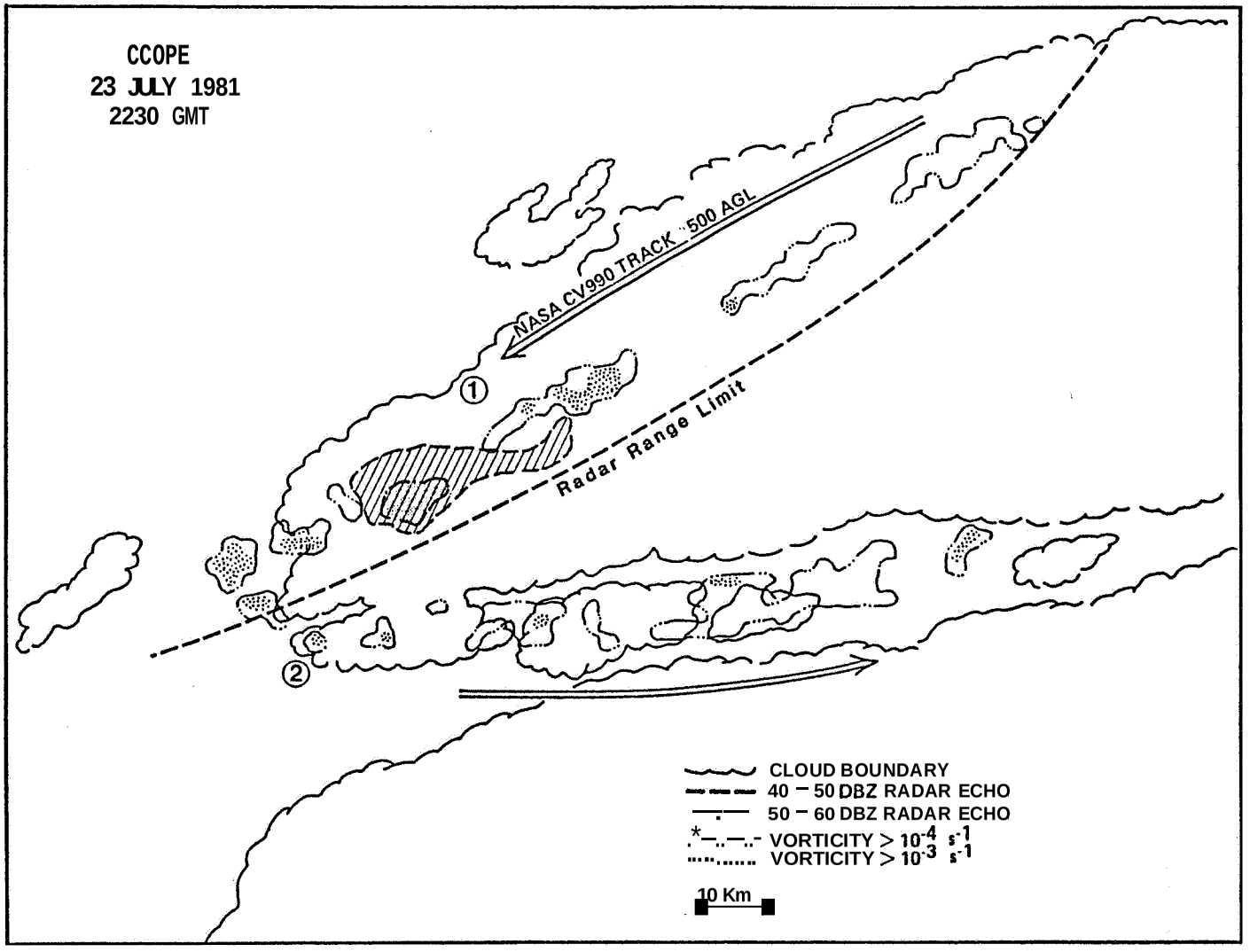

Fig. 36. Overlay of ADL wind vorticity field on the satellite derived cloud boundaries and the SWR-75 radar echo map. VORTICITY > 10^{-4} s^{-1} includes any values between 0.0 and 10^{-4} s^{-1}; > 10^{-3} s^{-1} includes any values between 0.0 and 10^{-3} s^{-1}--i.e. only zones of positive vorticity are plotted. Flight altitude is 500 m AGL.

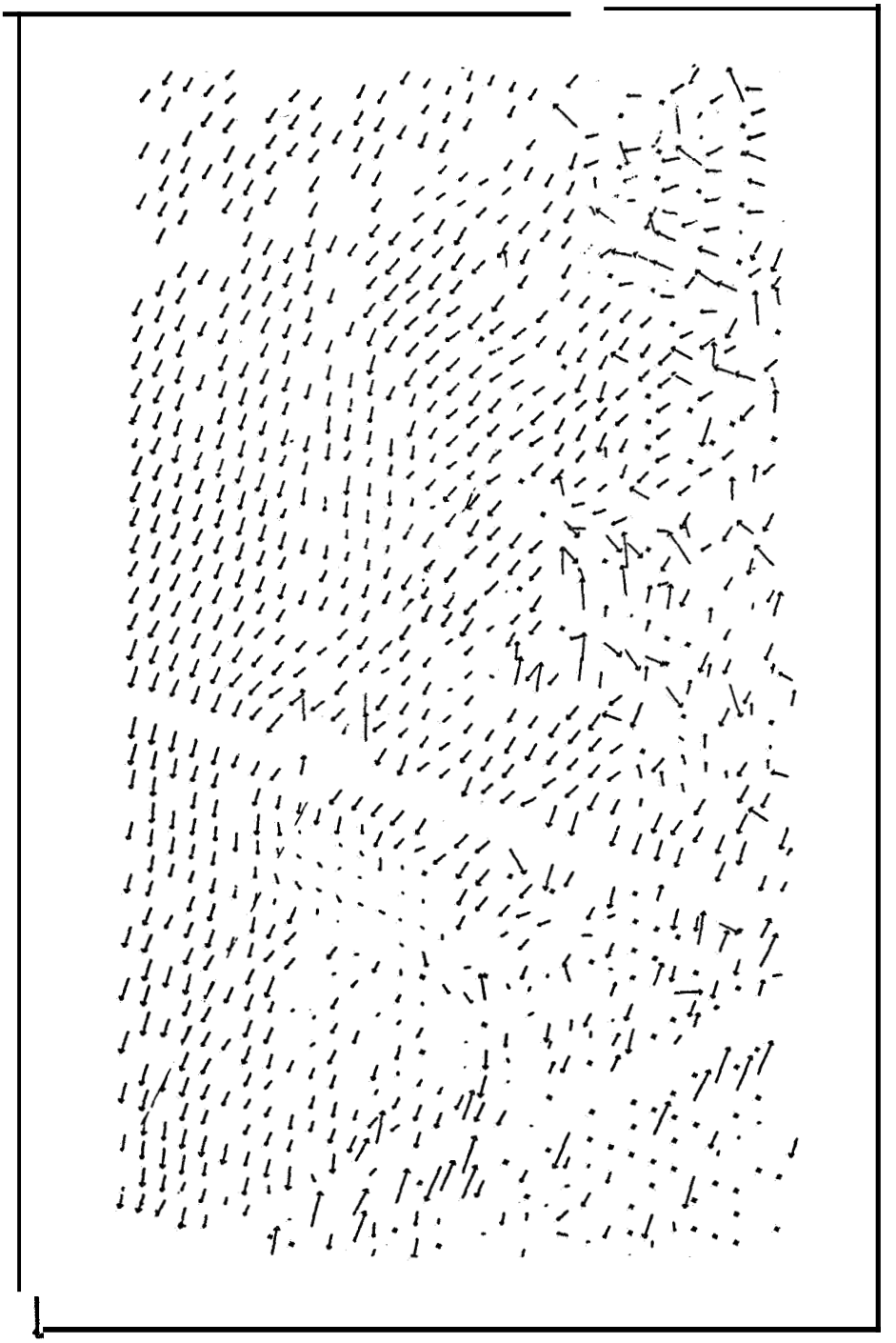

Fig. 37. Full resolution (330 m) wind vector field for region 1 noted in Figure 34.

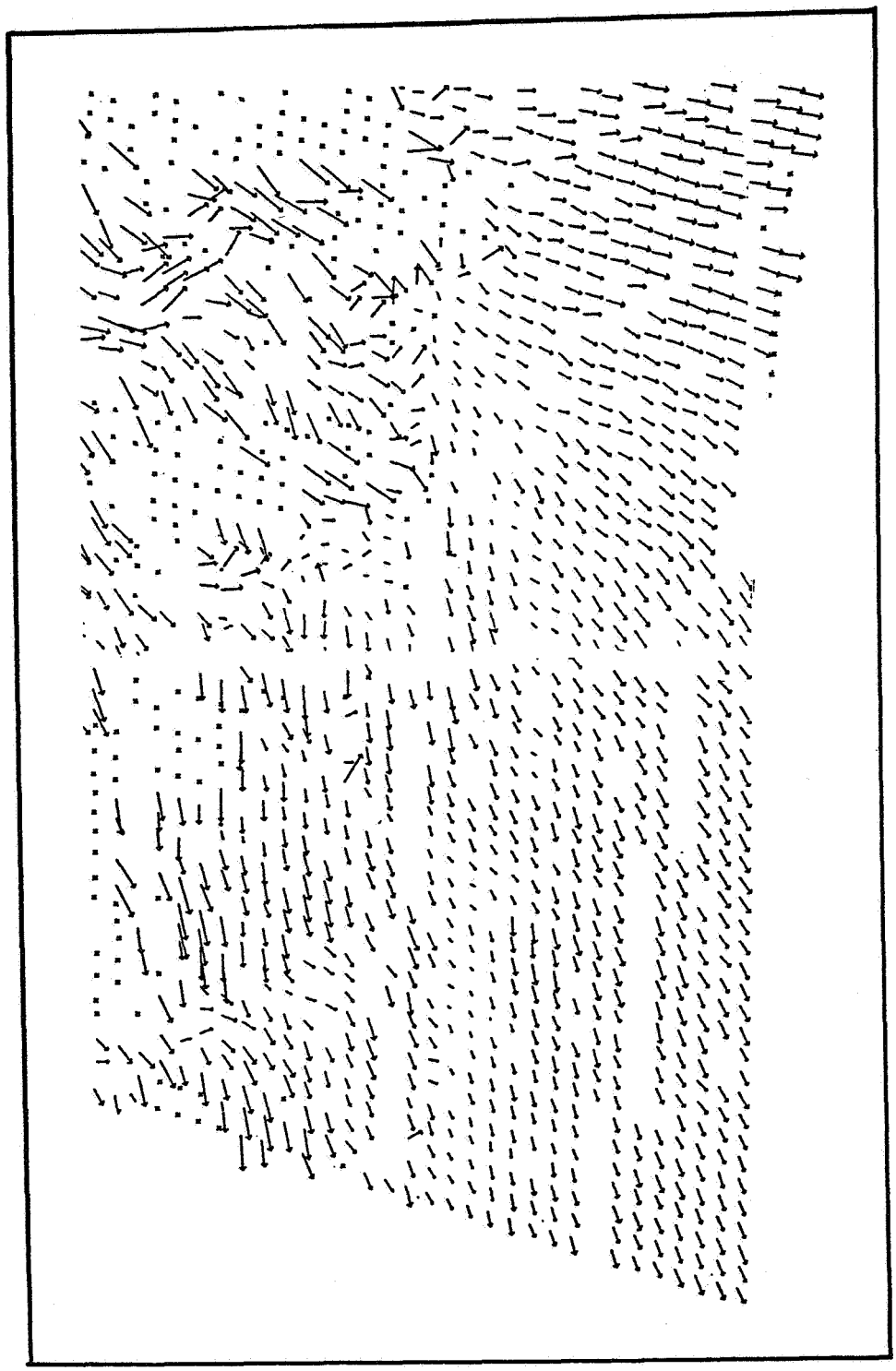

Fig. 38. Full resolution (330 m) wind vector field for region 2 noted in Figure 34.

4) the physical interpretation of atmospheric situations sampled by the ADLS is limited by the lack of thermal/moisture data with similar resolution and knowledge of the vertical context of the horizontal wind measurements;

5) however, the CCOPE ADLS data show that some outflows are organized with horizontal dimensions of 50-75 km even though the nearby radar echo fields show precipitation zones with 5-10 km dimensions;

6) on other occasions with similar satellite observed cloud type, size and organization, the general subcloud layer flow is characterized by many interacting features having 10-20 km horizontal dimensions; and

7) there is some suggestion that on occasion the stability of the outflow current may lead to a decoupling with the winds above it to the extent that the convergence patterns above the outflows (e.g. 600 m) are not aligned with those nearer the surface (e.g. 200 m).

In future programs where the ADLS is used to probe the atmosphere in the vicinity of deep convection, there should be an effort to obtain real-time satellite and radar products on board the aircraft to aid in navigating the aircraft to areas where outflows (or inflows) are most likely to be occuring. More time can be spent documenting the flows rather than searching for them.

4.0 REFERENCE

Bilbro, J., G. Fichtl, D. Fitzjarrald, M. Krause, and R. Lee, 1984. Airborne Doppler lidar wind field measurements, Bull. Amer. Met. Soc., 65, 348-359.

1. REPORT NO.	2. GOVERNMENT ACCESSION NO	3. RECIPIENT'S CATALOG NO.
NASA CR-3898		

4. TITLE AND SUBTITLE	5. REPORT DATE
Convective Storm Downdraft Outflows Detected by NASA/MSFC's Airborne 10.6 μm Pulsed Doppler Lidar System	May 1985
	6. PERFORMING ORGANIZATION CODE
7. AUTHOR(S) G. D. Emmitt	8. PERFORMING ORGANIZATION REPORT #
9. PERFORMING ORGANIZATION NAME AND ADDRESS Simpson Weather Associates, Inc. 809 East Jefferson Street Charlottesville, Virginia 22902	10. WORK UNIT NO. M-488
	11. CONTRACT OR GRANT NO. NAS8-35597
12. SPONSORING AGENCY NAME AND ADDRESS National Aeronautics and Space Administration Washington, DC 20546	13. TYPE OF REPORT & PERIOD COVERED Contractor Report July 30, 1984 - July 29, 85
	14. SPONSORING AGENCY CODE

15. SUPPLEMENTARY NOTES

Marshall Space Flight Center, Systems Dynamics Laboratory
Technical Monitors: Daniel E. Fitzjarrald, Margaret B. Alexander, and James W. Bilbro

The author conducted much of this work under the Universities Space Research Association's Visiting Scientist Program at the NASA/Marshall Space Flight Center, Huntsville, Alabama.

16. ABSTRACT

This document demonstrates the capability of a unique Airborne Doppler Lidar System to measure the horizontal winds in the vicinity of severe storm activity. The Airborne Doppler Lidar System (ADLS), developed at NASA/MSFC, was flown on a CV990 research aircraft during the CCOPE (Cooperative Convective Precipitation Experiments, Montana, Summer 1981). Flown between 400 and 600 m AGL, the lidar probed the subcloud regions of several deep convection storms.

ADLS data collected near storms on 21 and 23 July 1981 are presented along with satellite imagery, radar echo maps and surface station measurements. These case studies are evidence of the successful performance of an airborne remote wind sensing system and the advantages of two-dimension flow visualization of storm outflow structures and interactions.

17. KEY WORDS	18. DISTRIBUTION STATEMENT
Turbulence Atmospheric and Terrestrial Environmental Processes, Storm and Mesoscale Processes, Global Scale Processes	Unclassified - Unlimited STAR Category 47

19. SECURITY CLASSIF. (of this report)	20. SECURITY CLASSIF. (of this page)	21. NO. OF PAGES	22. PRICE
Unclassified	Unclassified	49	A03

For sale by National Technical Information Service, Springfield, Virginia 22161